PHYSICAL REVIEW D **87,** 023522 (2013)

Forecast constraints on cosmic strings from future CMB, pulsar timing, and gravitational wave direct detection experiments

Sachiko Kuroyanagi,[1] Koichi Miyamoto,[2] Toyokazu Sekiguchi,[3]
Keitaro Takahashi,[4] and Joseph Silk[5,6]

[1]*Research Center for the Early Universe (RESCEU), University of Tokyo, Tokyo 113-0033, Japan*
[2]*Institute for Cosmic Ray Research, University of Tokyo, Kashiwa 277-8582, Japan*
[3]*Department of Physics and Astrophysics, Nagoya University, Nagoya 464-8602, Japan*
[4]*Faculty of Science, Kumamoto University, 2-39-1, Kurokami, Kumamoto 860-8555, Japan*
[5]*Institut d' Astrophysique, 98bis Boulevard Arago, Paris 75014, France*
[6]*Department of Physics, University of Oxford, Keble Road, Oxford OX1 3RH, United Kingdom*

(Received 10 October 2012; published 24 January 2013)

We study future observational constraints on cosmic string parameters from various types of next-generation experiments: direct detection of gravitational waves (GWs), pulsar timing array, and the cosmic microwave background. We consider both GW burst and stochastic GW background searches by ground- and space-based interferometers as well as GW background detection in pulsar timing experiments. We also consider cosmic string contributions to the cosmic microwave background temperature and polarization anisotropies. These different types of observations offer independent probes of cosmic strings and may enable us to investigate cosmic string properties if the signature is detected. In this paper, we evaluate the power of future experiments to constrain cosmic string parameters, such as string tension $G\mu$, initial loop size α, and reconnection probability p, by performing Fisher information matrix calculations. We find that combining the information from the different types of observations breaks parameter degeneracies and provides more stringent constraints on the parameters. We also find future space-borne interferometers independently provide a highly precise determination of the parameters.

DOI: 10.1103/PhysRevD.87.023522 PACS numbers: 98.80.Cq, 04.30.Db, 98.70.Vc

I. INTRODUCTION

Cosmic strings are linear topological defects which are formed at spontaneous symmetry breaking (SSB) in the early Universe [1] (as a review, see Ref. [2]). Some inflation models based on superstring theory predict fundamental strings, D-strings and their bound states of cosmological length. Such stringy cosmic strings are called cosmic superstrings [3–5]. They form a complicated string network, which consists of infinite strings and closed loops, and may leave remarkable signatures in the universe through their nonlinear evolution. If their signals are observed, not only the existence of cosmic strings will be confirmed but their properties might be studied. This enables us to obtain implications for both the history of the Universe such as inflation or SSB, and for physics beyond the Standard Model of particle physics such as grand unified theory or superstring theory through the study of cosmic strings. Therefore, cosmic strings are important probes of both cosmology and particle physics, and we are motivated to study how the properties of cosmic strings can be determined by future experiments.

Various types of observational signatures of comic strings have been studied intensively. One of them is the gravitational wave (GW) [6–17]. The main source of GWs in the string network is cusps on loops.[1] A cusp is a highly Lorentz boosted region on a loop which appears $\mathcal{O}(1)$ times in an oscillation period of the loop and it emits a strong beam of GWs, which we call a "GW burst." The GW bursts can be detected in two different forms. One is "rare bursts," which are infrequent but strong enough to be detected alone. The other is a stochastic GW background, which consists of many small bursts overlapping each other [10,11]. In our previous paper [20], we studied how cosmic string parameters are determined by direct detection of GWs in future ground-based GW experiments, such as Advanced LIGO [21], Advanced Virgo [22] and KAGRA [23], and showed that measurements of the burst rate and the GW background provide different information and lead to better constraints on parameters when they are combined.

[1]Concerning the stochastic GW background, kinks make a contribution comparable with cusps [16], which we do not take into account in this paper. For cosmic superstrings each loop may have many kinks on itself, and in such a case GWs from kinks may dominate that from cusps both in the rate of rare bursts and the amplitude of the stochastic background [18,19]. However, such a contribution strongly depends on the fraction of loops with junctions. So we do not consider their contribution in this paper.

In this paper, we extend our previous study in two ways. First, in addition to the ground-based detectors, we consider other types of GW experiment, that is, direct detection by space-borne interferometers such as eLISA/NGO [24], BBO [25] or DECIGO [26], and observation of the GW background in pulsar timing experiments, such as Parkes PTA [27], EPTA [28,29], NANOGrav [30,31] or Square Kilometre Array (SKA) [32]. These different types of GW experiments provide different information, since each type of experiment has its best sensitivity at different frequency: $\sim 10^2$ Hz for ground-based detectors, $\sim 10^{-2}$ Hz for eLISA/NGO, $\sim 10^{-1}$ Hz for DECIGO and BBO, and $\sim 10^{-8}$ Hz for pulsar timing experiments. Gravitational waves in different frequency bands are emitted at different redshifts and carry information on cosmic strings living in different epochs of the Universe.

Second, we also take into account observation of the cosmic microwave background (CMB). Cosmic strings may induce temperature and polarization fluctuations in CMB through gravitational effects, which is also an important observational signature of cosmic strings and studied intensively (for example, see Refs. [33–47]). Although current CMB observations indicate that cosmic strings are not the dominant source of CMB fluctuations, the string signatures might be observed in small-scale fluctuations and/or B-mode polarization by future experiments such as Planck [48] and CMBpol [49]. Expected constraints on cosmic string parameters by these experiments are already studied in Ref. [50] by Fisher information matrix calculations. In this paper, we consider a combination of the constraints with GW experiments, which are expected to provide different information on cosmic strings.

As in Ref. [20], in this paper, we focus on three parameters which characterize cosmic string network. The first one is string tension μ, or the product of it and Newton constant G, $G\mu$. It represents the energy stored per unit length in a cosmic string. For the field theoretic string, it is comparable to the square of the energy scale of SSB, while for the cosmic superstring, it is determined by the energy scale of the superstring theory and the warp factor of the extra dimension where the string is located. The value of $G\mu$ affects not only the amplitudes of the GW bursts and GW background but also the spectral shapes through the change of the lifetime of loops. The amplitude of CMB fluctuations is also affected by the value of $G\mu$.

The second one is initial loop size α. The typical size of a loop at its formation is characterized by αt, where t is the time of the loop formation. In principle, the value of α can be predicted, if we can solve the nonlinear evolution of the string network, and there are many works which attempt to determine the value of α with numerical or analytical methods [51–63]. However, it is not yet clearly understood, so we treat α as a free parameter. The value of α affects both the GW burst rate and the GW background spectrum. On the other hand, the CMB signature is independent from α, since it is induced mainly by infinite strings and the contribution from loops is negligible.

The third one is reconnection probability p. For field theoretic strings, p is roughly equal to unity while for cosmic superstrings, it can be much smaller than 1. The string network becomes denser as p gets smaller. This leads to the enhancement of the burst rate, the GW background spectrum, and the CMB fluctuations. The shape of the CMB power spectrum is also affected, since the typical length scale of the string network becomes smaller and the average velocity of the strings becomes larger.

In this paper, we aim to investigate the abilities of the different types of experiments to constrain string parameters and study how they complement each other. We calculate the burst rate and the GW background spectrum using the formulation described in Ref. [20]. For CMB, we use CMBACT [64], which calculates the power spectrum by approximating the string network as an ensemble of randomly oriented straight segments [36]. Finally, we predict constraints on $G\mu$, α and p from the future experiments by performing Fisher matrix calculations and find that the different types of experiments break the degeneracies in the parameters and help to tighten the constraints when they are combined.

This paper is constructed as follows. In Sec. II, we briefly review the model to describe the cosmic string network and the methods to calculate GWs from string loops and CMB power spectra induced by strings. In Sec. III, we describe the sensitivities of current and future experiments and the Fisher matrix formalism for direct detection, pulsar timing, and CMB experiments. In Sec. IV, we first show the parameter space to be explored by these experiments, and then calculate constraints on the cosmic string parameters for three fiducial models. We summarize the paper in Sec. V. Throughout the paper, we use the cosmological parameters from the 7-year WMAP data (WMAP + BAO + H0 mean) [65]: the ratio of the present energy density of baryon to the critical density $\Omega_b h^2 = 0.02255$, that of cold dark matter $\Omega_c h^2 = 0.1126$, that of dark energy $\Omega_\Lambda = 0.725$, the spectral index of the primordial curvature perturbation $n_s = 0.968$, the reionization optical depth $\tau = 0.088$, the amplitude of the primordial curvature perturbation $\Delta^2_{\mathcal{R}}(k_0) = 2.43 \times 10^{-9}$ at $k_0 = 0.002\,\mathrm{Mpc}^{-1}$, Hubble constant $H_0 = 70.2\,\mathrm{km/s/Mpc}$ and the primordial helium abundance $Y_p = 0.326$.

II. CALCULATION OF VARIOUS TYPES OF COSMIC STRING SIGNATURES

In this section, we briefly mention how to calculate the observational signatures of cosmic strings. After explaining the analytic model of the cosmic string network, we describe the formalism to calculate the burst rate, the GW background spectrum and the CMB power spectrum and mention their dependence on string parameters.

A. The model of the cosmic string network

As in our previous paper [20], we adopt the model in Refs. [66,67], which is based on the velocity-dependent one-scale model [68]. The network of infinite strings is considered as a random walk with a correlation length ξ, which corresponds to the typical curvature radius and interval of infinite strings, and the total length L of infinite strings in volume V is given by $L = V/\xi^2$. The equations for $\gamma \equiv \xi/t$ and the root mean square velocity of infinite strings v are given by

$$\frac{t}{\gamma}\frac{d\gamma}{dt} = -1 + Ht + \frac{\tilde{c}(t)pv}{2\gamma} + Htv^2, \tag{1}$$

$$\frac{dv}{dt} = (1-v^2)H\left(\frac{k(v)}{Ht\gamma} - 2v\right), \tag{2}$$

where $k(v) = \frac{2\sqrt{2}}{\pi}\frac{1-8v^6}{1+8v^6}$ [69]. The Hubble parameter is given by

$$H(t) \equiv \frac{\dot{a}}{a} = H_0[\Omega_\Lambda + \Omega_m(1+z)^3 + \Omega_r(1+z)^4]^{1/2}, \tag{3}$$

where $a(t)$ is the scale factor, $1+z = a_0/a(t)$ is the redshift, a_0 is the present value of the scale factor, $\Omega_m = \Omega_b + \Omega_c$ and Ω_r is the ratio of the present energy density of radiation to the critical density. The parameter $\tilde{c}(t)$ represents the efficiency of loop formation. The value of this parameter between the radiation-dominated era and the matter-dominated era is interpolated by

$$\tilde{c}(t) = \frac{c_r + \frac{gc_m}{1+z}}{1+\frac{g}{1+z}}, \tag{4}$$

where we set $c_r = 0.23$, $c_m = 0.18$ and $g = 300$ according to Refs. [36,70]. With these values, the evolution of γ and v agrees with results from numerical simulations such as Ref. [68].

The parameters $\gamma(t)$ and $v(t)$ have different time evolutions depending on the Hubble expansion rate. In our previous paper, we used the asymptotic values for each radiation-dominated and matter-dominated Universe. However, in this paper, since we additionally investigate the effect on the CMB fluctuations, which are produced near the transition from the radiation-dominated to the matter-dominated Universe, we numerically solve Eqs. (1) and (2) to evaluate the values of $\gamma(t)$ and $v(t)$. Their initial values are determined by the solution of $d\gamma/dt = 0$ and $dv/dt = 0$ in the radiation-dominated era with $\tilde{c} = c_r$ and $Ht = 1/2$.

Figures 1(a) and 1(b) show the time evolutions of $\gamma(t)$ and $v(t)$ and their dependence on the reconnection probability p. For $p = 1$, γ and v reach the asymptotic values in the matter-dominated era from those in the radiation-dominated era by $z \sim 10^2$. After the dark energy becomes a dominant component of the universe at $z \lesssim 1$, γ begins to increase and v begins to decrease, because the exponential expansion of the universe dilutes strings and makes them slow down. For small p, we see the overall magnitude of γ decreases as p decreases, the dependence is proportional to p^{-1} and $p^{-1/2}$ for the radiation- and matter-dominated era, respectively, [20]. The asymptotic value of v is approximately $1/\sqrt{2}$ in both the radiation- and matter-dominated eras.

B. Gravitational waves from cosmic string loops

Here, we briefly describe the formalism to calculate GWs from cosmic strings. The detail is described in our previous paper [20], or originally in Refs. [10–13].

Since the main source of GWs in the string network is cusps on loops, we first evaluate the density of loops in the Universe in order to calculate GWs from them. In the scaling regime, where the typical length scale of infinite strings is proportional to the Hubble scale and their number in a Hubble horizon remains constant, infinite strings continuously convert their length into loops. The number density of loops formed at time t_i is given by

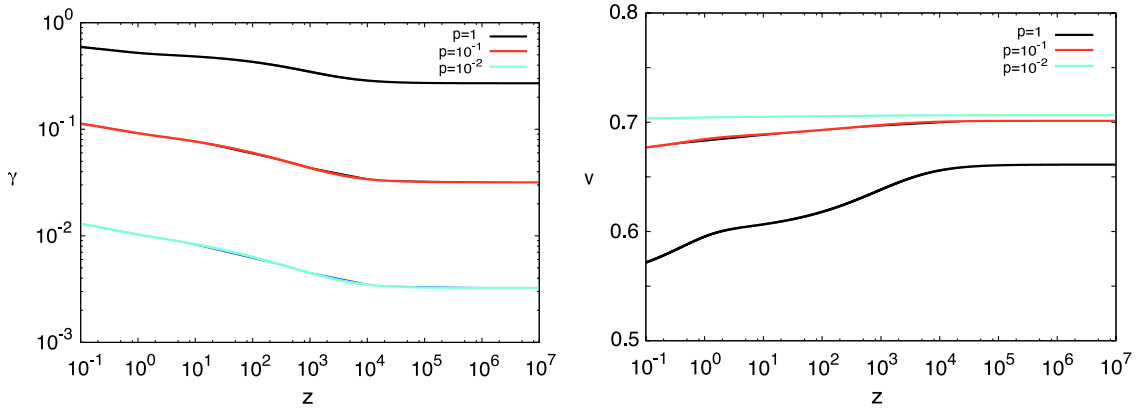

(a) γ for $p = 1, 10^{-1}, 10^{-2}$. (b) v for $p = 1, 10^{-1}, 10^{-2}$.

FIG. 1 (color online). The time evolution of γ and v for different values of p.

$$\frac{dn}{dt_i}(t,t_i)dt_i = \frac{dt_i}{\alpha\gamma(t_i)^2 t_i^4}\left(\frac{a(t_i)}{a(t)}\right)^3, \tag{5}$$

at time t. Loops continue to shrink by releasing energy as GWs and eventually evaporate. The length of a loop formed at t_i is given by

$$l(t,t_i) = \alpha t_i - \Gamma G\mu(t - t_i), \tag{6}$$

for time t. Here, Γ is a constant which represents the efficiency of the GW emission from loops and set to 50 in this paper. If $\alpha \gg \Gamma G\mu$, loops are long-lived, that is, they survive more than a Hubble time. On the other hand, if $\alpha \ll \Gamma G\mu$, loops are short-lived, and they evaporate within a Hubble time. Using Eqs. (5) and (6), we can describe the number density of loops in terms of length l and time t.

Cusps emit GWs of $f \gg l^{-1}$ into a small solid angle. The linearly polarized waveform of a GW burst emitted in a direction $\mathbf{n}$ by a loop with length l at redshift z is given by

$$h_{\mu\nu}(t,\mathbf{n}) = \int dfh(f,z,l)e^{-2\pi i f t}e^{+}_{\mu\nu}(\mathbf{n}) \times \Theta(\mathbf{n}\cdot\mathbf{n}_c - \cos[\theta_m(f,z,l)]) \times \Theta(1-\theta_m(f,z,l)), \tag{7}$$

where $\mathbf{n}_c$ is the direction of the center of the burst, θ_m is the beaming angle of the GW burst which is given by

$$\theta_m(f,z,l) = ((1+z)fl)^{-1/3}, \tag{8}$$

and $e^{+}_{\mu\nu} = l_\mu m_\nu - l_\nu m_\mu$ is the polarization tensor (for plus polarization), where $l_\mu = (0,\mathbf{l})$, $m_\mu = (0,\mathbf{m})$ and $\mathbf{l}$ and $\mathbf{m}$ are unit vectors orthogonal to $\mathbf{n}$ and each other. The Fourier transform of the GW amplitude, $h(f,z,l)$, is given by

$$h(f,z,l) \approx 2.68\frac{G\mu l}{((1+z)fl)^{1/3}r(z)f}, \tag{9}$$

where $r(z) = \int_0^z dz'/H(z')$. The first Heaviside step function Θ in Eq. (7) is introduced to account for the beaming of the GW and the second one is for the low frequency cutoff at $f \lesssim l^{-1}$.

The arrival rate of GW bursts with frequency f and amplitude h emitted at redshift z is given by

$$\frac{dR}{dzdh}(f,h,z) = \frac{3}{4}\theta_m^2(f,z,l)\frac{c}{(1+z)h}\frac{1}{\gamma(t_i)^2\alpha t_i^4} \times \frac{1}{\alpha+\Gamma G\mu}\left(\frac{a(t_i)}{a(t)}\right)^3\frac{dV}{dz} \times \Theta(1-\theta_m(f,z,l)), \tag{10}$$

where

$$\frac{dV}{dz}(z) = \frac{4\pi a^2(z)r^2(z)}{H(z)(1+z)}. \tag{11}$$

From Eqs. (6) and (9), l and t_i can be expressed as

$$l(f,h,z) = \left(\frac{hr(z)}{2.68G\mu}(1+z)^{1/3}f^{4/3}\right)^{3/2}, \tag{12}$$

$$t_i(f,h,z) = \frac{l(f,h,z)+\Gamma G\mu t(z)}{\alpha+\Gamma G\mu}, \tag{13}$$

which enables one to express Eq. (10) in terms of h, z, and f. Finally, the total arrival rate of GWs today for given frequency and amplitude is given by

$$\frac{dR}{dh} = \int_0^\infty dz\frac{dR}{dhdz}. \tag{14}$$

The GW bursts are identified as a single burst if they do not overlap each other. In contrast, bursts overlapping each other are observed as a GW background. Namely, a GW background is formed by bursts which come to the observer with a time interval shorter than the oscillation period of themselves. According to the criteria in Ref. [13], such bursts have amplitude smaller than h_*, which is determined for a given frequency as

$$\int_{h_*}^\infty dh\frac{dR}{dh} = f. \tag{15}$$

Then, the amplitude of a GW background, $\Omega_{\rm GW}(f) \equiv (d\rho_{\rm GW}/d\ln f)/\rho_{\rm cr}$, where $\rho_{\rm GW}$ is the energy density of the GWs and $\rho_{\rm cr}$ is the critical density of the universe, is given by

$$\Omega_{\rm GW}(f) = \frac{2\pi^2}{3H_0^2}f^3\int_0^{h_*} dhh^2\frac{dR}{dh}. \tag{16}$$

The main contribution to $\Omega_{\rm GW}$ at frequency f comes from loops expiring at the redshift which satisfies $\min\{\alpha,\Gamma G\mu\} \times t \sim f^{-1}(1+z)^{-1}$ in the radiation-dominated era or loops expiring recently.

Here, we briefly mention the parametric dependence of the burst rate and $\Omega_{\rm GW}$. The burst rate and the amplitude of the GW background are basically enhanced as $G\mu$ increases. However, the value of $G\mu$ also affects the spectral shape of the burst rate and GW background, since the number density of loops is affected by $G\mu$ through the lifetime of loops. This is important especially in the case of $G\mu > \alpha$, where $G\mu$ determines the size of expiring loops. The large value of α decreases the initial number density of loops. However, it also has an effect to increase the number density of loops, since large α makes the lifetime of loops longer. Therefore, the effects of α on the burst rate and the background depend on values of f, h and the other parameters. Larger p simply leads to a larger burst rate and larger amplitude of the background, through the factor γ^{-2} in Eq. (10). We refer to Ref. [20] for a more detailed discussion.

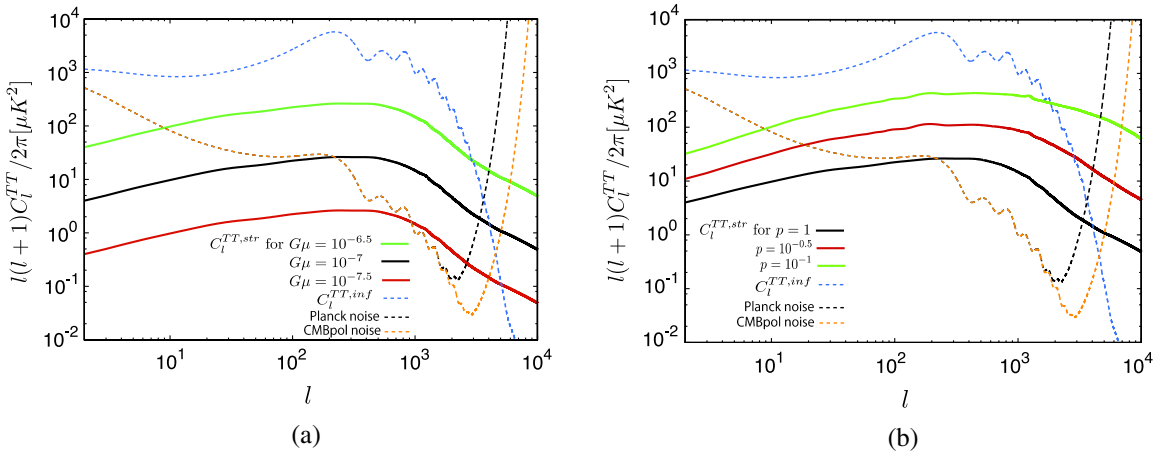

FIG. 2 (color online). (a) Dependence of the temperature spectrum on $G\mu$. The green, black and red solid lines represent the spectra for $G\mu = 10^{-6.5}$, $G\mu = 10^{-7}$ and $G\mu = 10^{-7.5}$, respectively, with p fixed to 1. (b) Dependence of the temperature spectrum on p. The black, red and green solid lines represent the spectra for $p = 1$, $p = 10^{-0.5}$ and $p = 10^{-1}$, respectively, with $G\mu$ fixed to 10^{-7}. The power spectra of CMB temperature fluctuations induced by strings for various parameter sets. In each figure, the black solid line represents the spectrum for the fiducial parameter set taken for the Fisher analysis in Sec. IV C. We also show the spectrum predicted by inflation as a blue dotted line and the expected noise levels for Planck and CMBpol as a black and an orange dotted line, respectively.

C. CMB fluctuations induced by cosmic strings

Here, we describe the method to calculate the power spectra of CMB fluctuations produced by cosmic strings. We refer to Refs. [36,64] for the details.

The evolution of the string network is highly nonlinear and produces all types of perturbations: scalar, vector and tensor modes. For the calculation of the CMB power spectra, we use a code based on CMBACT [64], which we modify to include the time evolution of γ and v. This code is based on the semianalytical method described in Ref. [36], which models the string network as an ensemble of discrete straight line segments. The length and the velocity of each segment are set to the solution of Eqs. (1) and (2). The position and the direction of the velocity are randomly selected for each segment. At each time step, some segments are removed so that the number density of strings is consistent with the scaling. Then, we can derive the energy-momentum tensor of such a simplified network and compute the power spectra of CMB fluctuations. In this paper, we assume that infinite strings have no wiggliness, which is introduced in Ref. [36].

Here, we briefly discuss the parametric dependencies of the CMB power spectra. A more detailed discussion is given in Ref. [42]. In Figs. 2 and 3, we show the CMB power spectra of temperature fluctuations $C_l^{\rm TT,str}$ and B-mode polarization $C_l^{\rm BB,str}$ induced by cosmic strings, respectively, for various parameter sets. We also show the temperature spectrum induced by the inflationary primordial perturbations $C_l^{\rm TT,inf}$ in Fig. 2, the B-mode polarization from the inflationary GWs $C_l^{\rm BB,inf}$ and that from the gravitational lensing of E-modes $C_l^{\rm BB,len}$ in Fig. 3, which are calculated by CAMB [71,72]. In addition, we plot the expected noise levels of Planck and CMBpol, which is given by the sum of the instrumental noise and the cosmic variance,

$$\frac{l(l+1)}{2\pi}N_{T;l}^{\rm tot} = \frac{l(l+1)}{2\pi}\sqrt{\frac{2}{(2l+1)l}}(C_l^{\rm TT,inf} + N_{T;l}), \qquad (17)$$

for temperature fluctuations, and

$$\frac{l(l+1)}{2\pi}N_{B;l}^{\rm tot} = \frac{l(l+1)}{2\pi}\sqrt{\frac{2}{(2l+1)l}}(C_l^{\rm BB,len} + N_{P;l}), \qquad (18)$$

for B-modes.[2] The instrumental noise spectra for the temperature $N_{T;l}$ and the polarization $N_{P;l}$ are defined in Sec. III.

The power spectrum of CMB temperature fluctuations induced by strings has a single bump, unlike the acoustic oscillations seen in the inflationary CMB power spectra. This is because strings generate fluctuations constantly and such fluctuations are incoherent, while the primordial fluctuations generated during inflation oscillate coherently. The peak of $C_l^{\rm TT,str}$ corresponds to the scale of the perturbations generated at last scattering. Another important difference is that $C_l^{\rm TT,str}$ does not decay exponentially as l increases in contrast to the Silk dumping of the inflationary spectrum at large l. This makes $C_l^{\rm TT,str}$ larger than $C_l^{\rm TT,inf}$ at

[2]The variance of C_l^i is given by $(\Delta C_l^i)^2 = \frac{2}{2l+1}(C_l^i + N_{a;l})^2$, where i denotes TT or BB and a denotes T or P. When we take a logarithmically homogeneous binning of l with bin width $\Delta \ln l = 1$, there are l multipoles in a bin at l. Since different multipoles are independent, the noise level per each bin should be given by $\Delta C_l^i/\sqrt{l}$. This allows us rough estimation of the detectability of the signal by eye in Figs. 2 and 3.

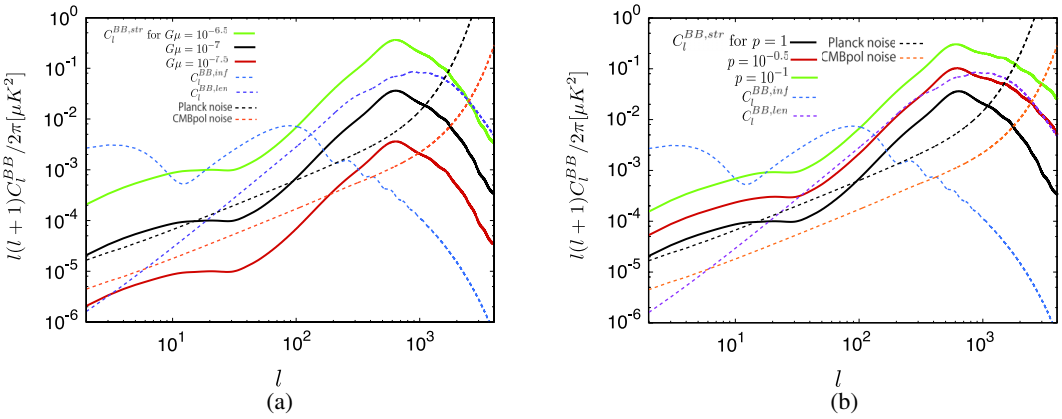

FIG. 3 (color online). (a) Dependence of the B-mode spectrum on $G\mu$. The green, black and red solid lines represent the spectra for $G\mu = 10^{-6.5}$, $G\mu = 10^{-7}$ and $G\mu = 10^{-7.5}$, respectively, with p fixed to 1. (b) Dependence of the B-mode spectrum on p. The black, red and green solid lines represent the spectra for $p = 1$, $p = 10^{-0.5}$ and $p = 10^{-1}$, respectively, with $G\mu$ fixed to 10^{-7}. The power spectra of CMB B-mode polarization induced by strings for various parameter sets. In each figure, the black solid line represents the spectrum for the fiducial parameter set taken in the Fisher analysis in Sec. IV C. The blue dotted line is the spectrum induced by the inflationary GWs. The tensor-to-scalar ratio r is set to 0.1. The purple dotted line is the spectrum of B-mode polarization generated through the gravitational lensing of the inflationary E-mode polarization. The black and the orange dotted lines represent the expected noise levels for Planck and CMBpol, respectively.

high l and it may be observable by future experiments.[3] The B-mode power spectrum also does not have oscillations, but has two bumps. The bump at high l and that at low l correspond to the polarization generated around the last scattering and around reionization, respectively. If the amplitude of the primordial gravitational wave is small, strings can be the main source of B-mode polarization.

The dependence of CMB power spectra on $G\mu$ is simple. The amplitudes of temperature and polarization fluctuations are proportional to $G\mu$, so the power spectra are proportional to $(G\mu)^2$. The effect of p arises through the correlation length of the string network γ and the rms velocity of strings v. For small p, γ becomes smaller and v becomes larger. If p is small, the small value of γ makes the string network denser and enhances the amplitude of the CMB fluctuations. Also, the small correlation length γ makes the typical scale of perturbations smaller. However, at the same time, large v makes the typical scale of perturbations larger [42]. Since the two effects on the typical scale of perturbations compensate, we find no apparent shift of the peak in Figs. 2 and 3 with the change of the value of p. While these effects tend to compensate, small effects are seen in the width of the peak and the slope of the small-scale spectrum.

Since the CMB anisotropy is induced not by loops but by infinite strings, the CMB power spectra do not depend on α.

[3]The power spectra of E-mode polarization $C_l^{\rm EE}$ and the cross correlation between temperature and E-mode $C_l^{\rm TE}$ by strings also decay more slowly than the inflationary spectrum at high l. However, they have small amplitude and do not affect the observation when we assume realistic parameters.

III. FORMALISM TO EVALUATE THE SENSITIVITY AND THE CONSTRAINTS ON PARAMETERS IN EACH EXPERIMENT

In this section, we describe the method to calculate the Fisher information matrix, which is used to estimate the power of each experiment to determine the string parameters. For GW burst and background detection by interferometers, Ref. [20] provides more detailed derivations.

Given a data set of experiments, the parameter values that are most likely to result in the model prediction are those which maximize the likelihood function $\mathcal{L}$. Such a method for parameter estimation is called the maximum likelihood method and widely used in the analysis of cosmological observations [73]. The error in this estimation can be predicted by calculating the Fisher information matrix

$$\mathcal{F}_{lm} \equiv -\frac{\partial^2 \ln \mathcal{L}}{\partial\theta_l \partial\theta_m}. \tag{19}$$

Assuming a Gaussian likelihood, the expected error in the parameter θ_l is given by

$$\sigma_{\theta_l} = \sqrt{(\mathcal{F}^{-1})_{ll}}. \tag{20}$$

A. GW burst detection

The search for GW burst signals from cosmic strings is performed by matched filtering [74,75], where we assume that the burst signal from a cosmic string cusp is linearly polarized and has the frequency dependence of $f^{-4/3}$. Then, the spectrum form is expressed by

$$h^+(f) = Af^{-4/3}\Theta(f_h - f)\Theta(f - f_l), \tag{21}$$

where the amplitude A can be read from Eq. (9). The low frequency cutoff f_l is given by the low frequency limit of the experiment and the high frequency cutoff f_h is typically given by the most sensitive frequency of the detector [76]. The signal to noise ratio (SNR) ρ is given by

$$\rho = \left[4\int_{f_l}^{f_h} df \frac{|\hat{h}(f)|^2}{S_n(f)}\right]^{1/2}, \tag{22}$$

where the GW signal $\hat{h}(f) = F^+h^+(f)$ is given by multiplying the detector response to plus polarized GWs F^+. Effectively, F^+ can be replaced with the all sky-averaged value for orthogonal arm detectors, $\bar{F}^+ \sim 1/\sqrt{5}$ for a single detector, or $\bar{F}^+ \sim 1$ for the GW detector network which has 100% visibility over the whole sky. The noise spectral density $S_n(f)$ is defined by $\langle n(f)^* n(f)\rangle \equiv S_n(f)\delta(f - f')/2$, where $n(f)$ is the Fourier transform of the detector noise $n(t)$ and $\langle\cdots\rangle$ denotes the ensemble average. In this paper, we take the detection threshold as $\rho > 4$ [10].

For current LIGO, the noise spectrum is given by

$$\begin{aligned} S_n(f) = {} & 1.09\times 10^{-41}\left(\frac{30\ \mathrm{Hz}}{f}\right)^{28} \\ & + 1.44\times 10^{-45}\left(\frac{100\ \mathrm{Hz}}{f}\right)^{4} \\ & + 1.28\times 10^{-46}\left(1 + \left(\frac{90\ \mathrm{Hz}}{f}\right)^{-2}\right)\mathrm{Hz}^{-1}, \end{aligned} \tag{23}$$

and we take $f_l = 40$ Hz and $f_h = 150$ Hz [74]. The detection threshold $\rho > 4$ corresponds to the detection limit $A \simeq 9.1\times 10^{-21}\ \mathrm{s}^{-1/3}$ or $fh \simeq 1.7\times 10^{-21}$ at $f = 150$ Hz. For the future ground-based GW detectors, such as Advanced LIGO, we use

$$S_n(f) = 10^{-49}\left[x^{-4.14} - \frac{5}{x^2} + 111\left(\frac{2 - 2x^2 + x^4}{2 + x^2}\right)\right]\mathrm{Hz}^{-1}, \tag{24}$$

where $x = f/(215\ \mathrm{Hz})$ [77], and we take $f_l = 10$ Hz and $f_h = 220$ Hz. If we consider a world-wide detector network and assume $\bar{F}^+ \sim 1$, the detection limit is $A \simeq 2.1\times 10^{-22}\ \mathrm{s}^{-1/3}$ or $fh \simeq 3.4\times 10^{-23}$ at $f = 220$ Hz. For eLISA/NGO, we use

$$S_n(f) = \frac{20}{3}\frac{4S_{\mathrm{acc}} + S_{\mathrm{sn}} + S_{\mathrm{omn}}}{L^2}\left(1 + \left(\frac{f}{0.41(\frac{c}{2L})}\right)^2\right), \tag{25}$$

where $S_{\mathrm{acc}} = 1.37\times 10^{-32}(1 + \frac{10^{-4}\ \mathrm{Hz}}{f})f^{-4}\ \mathrm{m^2\,s^{-4}\,Hz^{-1}}$, $S_{\mathrm{sn}} = 5.25\times 10^{-23}\mathrm{m^2 Hz^{-1}}$ and $S_{\mathrm{omn}} = 6.28\times 10^{-23}\mathrm{m^2 Hz^{-1}}$ with the arm length $L = 1.0\times 10^6$ km [24], and take $f_l = 10^{-6}$ Hz and $f_h = 7.0\times 10^{-3}$ Hz. Then, the detection limit is $A \simeq 8.9\times 10^{-22}\ \mathrm{s}^{-1/3}$ or $fh \simeq 5.8\times 10^{-21}$ at $f = 7.0\times 10^{-3}$ Hz. For BBO or DECIGO, whose sensitivities are roughly the same, we use the configuration of BBO. It is designed to use a technique called time-delay interferometry (TDI), and the noise spectrum is given by

$$S_n(f) = \left(\frac{R_A(f)}{S_A(f)} + \frac{R_E(f)}{S_E(f)} + \frac{R_T(f)}{S_T(f)}\right)^{-1}. \tag{26}$$

The subscripts (A, E, T) denote the TDI variables and each noise spectrum is given by

$$\begin{aligned} S_A(f) &= S_E(f) \\ &= 8\sin^2(\hat{f}/2)[(2 + \cos\hat{f})S_{\mathrm{shot}} \\ &\quad + 2(3 + 2\cos\hat{f} + \cos(2\hat{f}))S_{\mathrm{accel}}], \\ S_T(f) &= 2[1 + 2\cos\hat{f}]^2[S_{\mathrm{shot}} + 4\sin^2(\hat{f}/2)S_{\mathrm{accel}}], \end{aligned} \tag{27}$$

where $S_{\mathrm{shot}} = 2.0\times 10^{-40}/(L/\mathrm{km})^{-2}\ \mathrm{Hz}^{-1}$ and $S_{\mathrm{accel}} = 9.0\times 10^{-40}/(2\pi f/\mathrm{Hz})^{-4}/(2L/\mathrm{km})^{-2}\ \mathrm{Hz}^{-1}$ with the arm length $L = 5.0\times 10^4$ km. For the calculation of the detector response $R_{A,E,T}$, see Ref. [78]. We take $f_l = 0.1$ Hz and $f_h = 0.25$ Hz, where the low-frequency cutoff is determined to take into account the confusion noise from white dwarf binaries. This leads to the detection limit $A \simeq 1.2\times 10^{-24}\ \mathrm{s}^{-1/3}$ or $fh \simeq 1.9\times 10^{-24}$ at $f = 0.25$ Hz.

Let us suppose that we detect a sufficient number of GW bursts at f_{best}, at which the detector is most sensitive. Under the assumption that the number of bursts follows a Poisson distribution [79–81], the Fisher matrix is given by

$$\mathcal{F}_{lm} = \int_{h_{\min}}^{\infty} \frac{\partial\Phi}{\partial\theta_l}\frac{\partial\Phi}{\partial\theta_m}\frac{1}{\Phi}dh, \tag{28}$$

where $\Phi(h) \equiv dR/dh \times T$, which is a function of the model parameters, T is the observation time and $h_{\min}$ is the smallest amplitude of the detectable burst at $f = f_{\mathrm{best}}$.

B. Search for the stochastic GW background by interferometers

The GW background is searched by correlating output signals of two or multiple interferometers. The SNR in such a correlation analysis with N detectors is given by [82,83]

$$\rho = \left[\sum_{I=1}^{N}\sum_{J<I}^{N}\rho_{IJ}^2\right]^{1/2}, \tag{29}$$

where

$$\rho_{IJ} = \frac{2}{5}\sqrt{2T}\left[\int_0^\infty df \frac{S_h(f)^2|\gamma_{IJ}(f)|^2}{R_{IJ}(f)}\right]^{1/2}, \tag{30}$$

$$\begin{aligned} R_{IJ}(f) = {} & \left(\frac{2}{5}\right)^2 S_h(f)^2(|\gamma_{IJ}(f)|^2 + \gamma_{II}\gamma_{JJ}) \\ & + \frac{2}{5}S_h(f)(\gamma_{II}(f)S_{n,J}(f) + \gamma_{JJ}S_{n,I}(f)) \\ & + S_{n,I}(f)S_{n,J}(f), \end{aligned} \tag{31}$$

and T is the observation time. The subscripts I and J refer to independent signals obtained at each detector or TDI variables (A, E, T). The overlap reduction function between the Ith and Jth detector γ_{IJ} is given by

$$\gamma_{IJ}(f) \equiv \frac{5}{8\pi}\int d\hat{\mathbf{\Omega}}(F_I^+(f,\hat{\Omega})F_J^+(f,\hat{\Omega}) + F_I^\times(f,\hat{\Omega})F_J^\times(f,\hat{\Omega}))e^{-2\pi i f\hat{\mathbf{\Omega}}\cdot(\mathbf{x}_I-\mathbf{x}_J)}, \quad (32)$$

where F_I^+ or $F_I^\times$ is the detector response to plus or cross polarized GWs of the Ith detector, $\mathbf{x}_I$ is the position of the Ith detector and $\hat{\Omega}$ is the direction of GWs. We calculate γ_{IJ} following the procedure given in Ref. [84] for ground-based detectors and Ref. [85] for BBO. The signal spectrum can be corresponded to $\Omega_{\rm GW}$ as

$$S_h(f) = \frac{3H_0^2}{4\pi^2 f^3}\Omega_{\rm GW}(f). \quad (33)$$

In the weak signal approximation, $S_h(f) \ll S_{n,I}(f)$, Eq. (30) reduces to

$$\rho_{IJ} \simeq \frac{3H_0^2}{10\pi^2}\sqrt{2T}\left[\int_0^\infty df\frac{|\gamma_{IJ}(f)|^2\Omega_{\rm GW}(f)^2}{f^6 S_{n,I}(f)S_{n,J}(f)}\right]^{1/2}. \quad (34)$$

The weak signal approximation is valid for $\rho \lesssim 200$ [83,86].

From the nondetection of GW background, we can put an upper limit on $\Omega_{\rm GW}$. Current LIGO detectors set an upper bound of $\Omega_{\rm GW} < 7.2\times10^{-6}$ for 41.5 Hz $< f <$ 169.25 Hz, assuming a flat spectrum. A 3-year run of the future detector network including Advanced LIGO, Advanced Virgo and KAGRA, would reach $\Omega_{\rm GW} = 4.5\times10^{-9}$ at 10 Hz $< f <$ 200 Hz. A 3-year run of BBO/DECIGO would provide $\Omega_{\rm GW} = 9.2\times10^{-17}$ for 0.1 Hz $< f <$ 10 Hz. Since eLISA/NGO is designed to have only one independent channel, we do not consider the cross correlation analysis in eLISA/NGO.

The Fisher matrix for the GW background measurement is generally given by

$$\mathcal{F}_{lm} = \sum_{I=1}^{N}\sum_{J<I}^{N}\frac{8T}{25}\int_0^\infty df\frac{|\gamma_{IJ}(f)|^2\partial_{\theta_l}S_h(f)\partial_{\theta_m}S_h(f)}{R_{IJ}(f)}. \quad (35)$$

Under the weak signal approximation, it reduces to [86,87]

$$\mathcal{F}_{lm} = \left(\frac{3H_0^2}{10\pi^2}\right)^2 2T\sum_{I=1}^{N}\sum_{J<I}^{N} \times\int_0^\infty df\frac{|\gamma_{IJ}(f)|^2\partial_{\theta_l}\Omega_{\rm GW}(f)\partial_{\theta_m}\Omega_{\rm GW}(f)}{f^6 S_{n,I}(f)S_{n,J}(f)}. \quad (36)$$

C. Search for the stochastic GW background in pulsar timing experiments

Pulsar timing experiments provide a unique opportunity to observe GWs in low-frequency band 10^{-9}–10^{-7} Hz [88–90] (for a review, see Ref. [91]). The analysis is based on the measurement of pulse time-of-arrival (TOA) variations. The stochastic GW background causes fluctuations in the TOAs. One can extract the signal from noise associated with individual pulsars by correlating TOAs between different pulsars.

We follow the formalism described in Ref. [92] to calculate the SNR and the Fisher matrix for detection of GWs in pulsar timing experiments. Let us assume observations of $M \gg 1$ pulsars at time $t_0, t_1, \ldots, t_{N-1}$ with the time interval Δt. The total observation time is $T = N\Delta t$ and $N \gg 1$. Then, we can make $N_p = M(M-1)/2$ pulsar pairs from M pulsars. We denote the timing residual of ith pulsar at time t_a as $R_i(t_a)$. The correlation coefficient of ith pair is defined as

$$r_i \equiv \frac{1}{N}\sum_{a=0}^{N-1} R_{i_1}(t_a)R_{i_2}(t_a), \quad (37)$$

where i_1 and i_2 are the numbers allocated to the first and second pulsar in the ith pair. Under the existence of the isotropic stochastic GW background, the ensemble average of r_i is [93]

$$\langle r_i\rangle = \sigma_g^2\zeta(\theta_i), \quad (38)$$

where σ_g is the root mean square of the timing residuals induced by the GW background and given by

$$\sigma_g^2 = \int_{f_l}^{f_h} P_R(f)df. \quad (39)$$

The highest and lowest frequency of GWs is given by $f_h = 1/2\Delta t$ and $f_l = 1/T$. The power spectrum of the timing residuals P_R is defined as $\langle R_i(f)R_i(f')\rangle = P_R(f)\delta(f-f')/2$ and that induced by the GW background is given by

$$P_R(f) = \frac{H_0^2}{8\pi^4 f^5}\Omega_{\rm GW}(f). \quad (40)$$

Note that r_i induced by the GW background has a specific dependence on the angle between the direction to i_1th and i_2th pulsars, θ_i. This dependence is characterized by $\zeta(\theta_i)$, which is described as

$$\zeta(\theta) = \frac{3}{2}x\ln x - \frac{x}{4} + \frac{1}{2}(1+\delta(x)), \qquad x = \frac{1-\cos\theta}{2},$$
$$\delta(x) = \begin{cases} 1; & \text{for } x = 0 \\ 0; & \text{otherwise.} \end{cases} \quad (41)$$

The signature of the GW background can be extracted by calculating the following quantity:

$$S = \frac{\frac{1}{N_p}\sum_{i=0}^{N_p-1}(r_i - \bar{r})(\zeta(\theta_i) - \bar{\zeta})}{\sigma_r \sigma_\zeta}, \tag{42}$$

where $\bar{r}$ and $\bar{\zeta}$ are the arithmetic mean over all pairs of pulsars, and σ_r^2 and σ_ζ^2 are the sample variance of r and ζ. We define this quantity as a "signal." If pulsars are distributed isotropically, $\bar{\zeta} = 0$ and $\sigma_\zeta^2 = 1/\sqrt{48}$. Hereafter, we replace $\bar{\zeta}$ and σ_ζ^2 by these values. The ensemble average of S is given by

$$\langle S \rangle = \frac{\sigma_g^2 \sigma_\zeta}{\sqrt{\sigma_g^4 \sigma_\zeta^2 + \sigma_{\Delta r}^2}}, \tag{43}$$

where

$$\sigma_{\Delta r}^2 = \frac{1}{N_p}\sum_{i=0}^{N_p-1}\langle (r_i - \langle r_i \rangle)^2 \rangle. \tag{44}$$

If there is no correlation between data of different pulsars, $\langle r_i \rangle = 0$, S follows a Gaussian distribution with zero mean and variance $1/N_p$. Therefore, we define the SNR as $\rho \equiv \langle S \rangle \sqrt{N_p}$.

We assume that the noise of each pulsar is white and uncorrelated with that of the other pulsar and the signal of GWs. We also assume that all pulsars have the same noise and denote the root mean square of time residuals induced by noise as σ_n. Then, the SNR becomes

$$\rho = \sqrt{\frac{M(M-1)/2}{1 + [\chi(1+\bar{\zeta}^2) + 2(\sigma_n/\sigma_g)^2 + (\sigma_n/\sigma_g)^4]/N\sigma_\zeta^2}}, \tag{45}$$

where

$$\chi = \frac{1}{N\sigma_g^4}\sum_{a=0}^{N-1}\sum_{b=0}^{N-1} c_{ab}^2, \qquad c_{ab} = \langle R_i(t_a) R_i(t_b) \rangle. \tag{46}$$

Assuming that $P_R(f)$ is the monotonically decreasing function of f, the SNR can be enhanced by low-pass filtering and whitening, which modifies the SNR to [92]

$$\tilde{\rho} = \sqrt{\frac{M(M-1)/2}{1 + \tilde{\sigma}_{\Delta r}^2/\tilde{\sigma}_g^4 \sigma_\zeta^2}}, \tag{47}$$

where

$$\begin{aligned} \tilde{\sigma}_g^2 &= \frac{2}{N}\sigma_d^2 \sum_{i=1}^{N_{\max}} \frac{P_R(i)}{P_d(i)}, \\ \tilde{\sigma}_{\Delta r}^2 &= \frac{2\sigma_d^4}{N^2}\sum_{i=1}^{N_{\max}}\left(1 + \left(\frac{P_R(i)}{P_d(i)}\right)^2 \bar{\zeta}^2\right). \end{aligned} \tag{48}$$

Here, we define the discrete power spectra for the ith frequency bin as

$$\begin{aligned} P_g(i) &\equiv \int_{f_i}^{f_{i+1}} df P_R(f), \\ P_n(i) &\equiv \int_{f_i}^{f_{i+1}} df P_n(f) = \frac{2\sigma_n}{N}, \\ P_d(i) &\equiv P_g(i) + P_n(i), \end{aligned} \tag{49}$$

where

$$f_i = \begin{cases} \frac{0.97}{T}; & \text{for } i = 1 \\ \frac{i-0.5}{T}; & \text{for } i > 1. \end{cases} \tag{50}$$

The summation is carried out only over the frequency bins in which the GW signal dominates the noise, $P_g(i) > P_n$, and we define $N_{\max}$ as the number of the highest frequency bin.

Since we use the discrete power spectra and $N_{\max}$ is discrete, the SNR given in Eq. (47) is a discontinuous function of model parameters. This is inevitable as long as the TOA data are sampled at discrete time intervals. However, for the Fisher matrix calculation, we replace the equations by the expression of the continuous power spectrum,

$$\hat{\rho} = \sqrt{\frac{M(M-1)/2}{1 + \hat{\sigma}_{\Delta r}^2/\hat{\sigma}_g^4 \sigma_\zeta^2}}, \tag{51}$$

$$\hat{\sigma}_g^2 = \frac{\sigma_d^2}{f_h - f_l}\int_{f_l}^{f_{\max}} df \frac{P_R(f)}{P_n(f)}, \tag{52}$$

$$\hat{\sigma}_{\Delta r}^2 = \frac{\sigma_d^4}{N(f_h - f_l)}\int_{f_l}^{f_{\max}} df\left[1 + \left(\frac{P_R(f)}{P_n(f)}\right)^2 \bar{\zeta}^2\right]. \tag{53}$$

Here, $f_{\max}$ is given by $P_R(f_{\max}) = P_n(f_{\max})$. Then, Eq. (51) becomes a smooth function of the parameters, and is a good approximation of Eq. (47) for $N_{\max} \gg 1$. Using Eq. (51), we can calculate the Fisher matrix as

$$\mathcal{F}_{ij} = \frac{1}{N^2}\frac{\partial S}{\partial \theta_i}\frac{\partial S}{\partial \theta_j}, \tag{54}$$

where $S = (1 + \hat{\sigma}_{\Delta r}^2/\hat{\sigma}_g^4 \sigma_\zeta^2)^{-1/2}$ and $N = (M(M-1)/2)^{-1/2}$. If the interval of the discontinuity in Eq. (47) is much smaller than the error width derived from the Fisher matrix Eq. (54), it is consistent to approximate Eq. (47) by Eqs. (51) and (54) provides a good prediction. This is the case in our fiducial model investigated in the next section.

In this paper, we consider SKA, the future radio telescope array which is expected to discover a large number of pulsars and observe pulses with high accuracy, and take the parameters as $N = 500$, $M = 100$, $\sigma_n = 50$ ns, $T = 10$ years, according to Ref. [94]. The detection threshold is taken as $\rho > 4$ again. NANOGrav, one of the latest experiments, has placed the upper bound of the GW background, $\Omega_{\rm GW} < 1.9 \times 10^{-8}$ for $f \simeq 1/(5\ \text{years}) = 6.3 \times 10^{-9}$ Hz,

under the assumption that $\Omega_{\rm GW}$ has a power-law spectrum [31].

D. Measurement of CMB fluctuation

The Fisher matrix for measurement of CMB fluctuation is given by [95]

$$\mathcal{F}_{ij} = \sum_l \sum_{X,X'} \frac{\partial C_l^X}{\partial \theta_i} \mathrm{Cov}^{-1}(C_l^X, C_l^{X'}) \frac{\partial C_l^{X'}}{\partial \theta_j}, \tag{55}$$

where X and X' are summed over the temperature (TT), E-mode polarization (EE), B-mode polarization (BB) and cross correlation between temperature and E-mode (TE). Cov is the covariance matrix and given by

$$\begin{aligned}
\mathrm{Cov}(C_l^{\rm TT}, C_l^{\rm TT}) &= \frac{2}{(2l+1)f_s}(C_l^{\rm TT} + N_{T;l})^2, \\
\mathrm{Cov}(C_l^{\rm EE}, C_l^{\rm EE}) &= \frac{2}{(2l+1)f_s}(C_l^{\rm EE} + N_{P;l})^2, \\
\mathrm{Cov}(C_l^{\rm BB}, C_l^{\rm BB}) &= \frac{2}{(2l+1)f_s}(C_l^{\rm BB} + N_{P;l})^2, \\
\mathrm{Cov}(C_l^{\rm TE}, C_l^{\rm TE}) &= \frac{2}{(2l+1)f_s} \\
&\quad \times [(C_l^{\rm TE})^2 + (C_l^{\rm TT} + N_{T;l})(C_l^{\rm EE} + N_{P;l})], \\
\mathrm{Cov}(C_l^{\rm TT}, C_l^{EE}) &= \frac{2}{(2l+1)f_s}(C^{\rm TE})^2, \\
\mathrm{Cov}(C_l^{\rm TT}, C_l^{\rm TE}) &= \frac{2}{(2l+1)f_s} C_l^{\rm TE}(C_l^{\rm TT} + N_{T;l}), \\
\mathrm{Cov}(C_l^{\rm EE}, C_l^{\rm TE}) &= \frac{2}{(2l+1)f_s} C_l^{\rm TE}(C_l^{\rm EE} + N_{P;l}), \\
\mathrm{Cov}(C_l^{\rm TT}, C_l^{\rm BB}) &= \mathrm{Cov}(C_l^{\rm EE}, C_l^{\rm BB}) = \mathrm{Cov}(C_l^{\rm TE}, C_l^{\rm BB}) = 0,
\end{aligned} \tag{56}$$

where f_s denotes the sky coverage and is set 0.65 for both Planck and CMBpol in this paper. The noise power spectrum $N_{T,P;l}$ is given by [96]

$$\begin{aligned}
N_{T,P;l} &= \left[\sum_i (N_{T,P;l}^{(i)})^{-1}\right]^{-1}, \\
N_{T,P;l}^{(i)} &= (\theta_{\rm FWHM}^{(i)} \sigma_{T,P}^{(i)})^2 \exp\left(l(l+1)\frac{(\theta_{\rm FWHM}^{(i)})^2}{8\ln 2}\right),
\end{aligned} \tag{57}$$

TABLE I. Survey parameters adopted in our analysis for Planck. The values are taken from Ref. [48].

Bands [GHz]	$\theta_{\rm FWHM}$ [arcmin]	σ_T [μK]	σ_P [μK]
70	14.0	4.7	6.7
100	10.0	2.5	4.0
143	7.1	2.2	4.2
217	5.0	4.8	9.8

TABLE II. Survey parameters adopted in our analysis for CMBpol. The values are taken from Ref. [49].

Bands [GHz]	$\theta_{\rm FWHM}$ [arcmin]	σ_T [μK]	σ_P [μK]
45	17	5.85	8.27
70	11.0	2.96	4.19
100	8.0	2.29	3.24
150	5	2.21	3.13
220	3.5	3.39	4.79

where $\theta_{\rm FWHM}^{(i)}$ is the full width at half maximum of the Gaussian beam and $\sigma_{T,P}^{(i)}$ is the root mean square of the instrumental noise per pixel for temperature or polarization, for the ith frequency band. The frequency bands and parameter values are provided in Tables I and II for Planck and CMBpol, respectively.

The current limit on $G\mu$ from CMB experiments is derived in Ref. [97] using WMAP and South Pole Telescope data [98]. Their analysis provides the limit of $f_{\rm str} < 0.0175$, where

$$\begin{aligned}
f_{\rm str} &\equiv \frac{\sigma_{\rm str}^2}{\sigma_{\rm inf}^2}, \qquad \sigma_{\rm str}^2 = \sum_{l=2}^{2000} \frac{2l+1}{4\pi} C_l^{\rm TT,str}, \\
\sigma_{\rm inf}^2 &= \sum_{l=2}^{2000} \frac{2l+1}{4\pi} C_l^{\rm TT,inf}.
\end{aligned} \tag{58}$$

We find this constraint corresponds in our model to $G\mu < 1.4 \times 10^{-7}$ for $p = 1$, $G\mu < 3.6 \times 10^{-8}$ for $p = 10^{-1}$ and $G\mu < 1.0 \times 10^{-8}$ for $p = 10^{-2}$.[4]

Future experiments will improve the limit for $G\mu$ by measuring the B-mode. The minimum value of $G\mu$ reachable by the B-mode measurement can be estimated by $\sqrt{\sigma_{(G\mu)^2}}$ [39], where

$$\sigma_{(G\mu)^2}^{-2} = f_s \sum_l \frac{2l+1}{2} (C_l^{\rm BB,res} + N_{P;l})^{-2} \left(\frac{C_l^{\rm BB,str}}{(G\mu)^2}\right)^2, \tag{59}$$

and $C_l^{\rm BB,res}$ is the residual noise of $C_l^{\rm BB}$ after removing the contamination from the foregrounds. For the case where the lensing effect is not removed, $C_l^{\rm BB,res} = C_l^{\rm BB,len}$, we can probe $G\mu > 2.4 \times 10^{-8}$ for $p = 1$, $G\mu > 8.0 \times 10^{-9}$ for $p = 10^{-1}$, and $G\mu > 2.6 \times 10^{-9}$ for $p = 10^{-2}$ by Planck, and $G\mu > 1.2 \times 10^{-8}$ for $p = 1$, $G\mu > 3.9 \times 10^{-9}$ for $p = 10^{-1}$, and $G\mu > 1.2 \times 10^{-9}$ for $p = 10^{-2}$ by CMBpol. Even if we consider the case where the lensing effect is perfectly removed, $C_l^{\rm BB,res} = 0$, the above values are not improved significantly, because the instrumental noise we assume here is larger than the lensing noise, $C_l^{\rm BB,len} \ll N_{P;l}$.

[4]Note that the string network model assumed in Ref. [97] is different from that in this paper. This causes a small difference in the shape of the CMB spectrum. We neglect this difference and apply their constraint on $f_{\rm tsr}$ to our model.

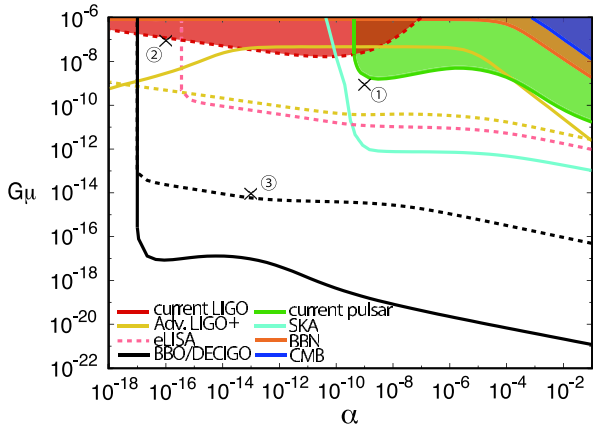

(a) $p = 1$

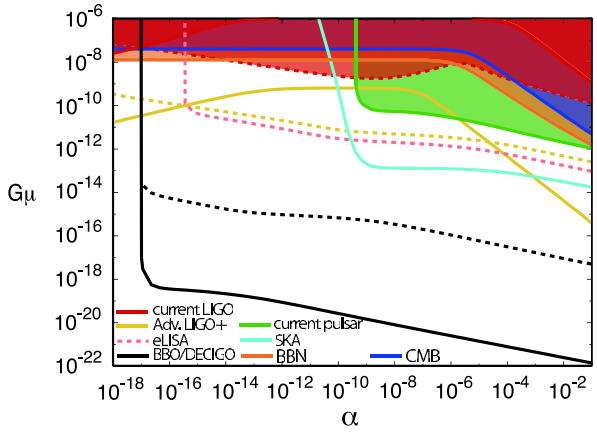

(b) $p = 10^{-1}$

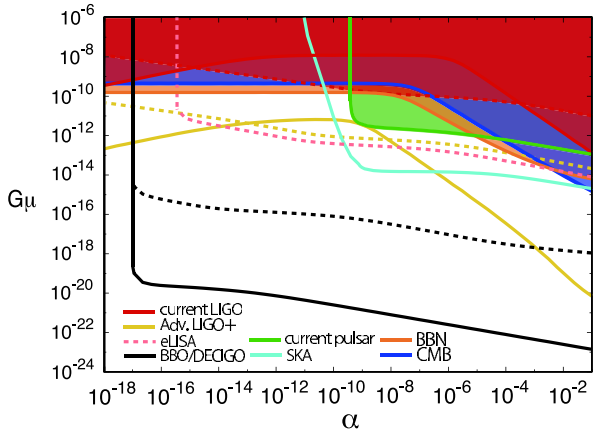

(c) $p = 10^{-2}$

FIG. 4 (color online). Accessible parameter space in the $G\mu$-α plane for $p = 1$, $p = 10^{-1}$ and $p = 10^{-2}$. The colored regions are excluded by current experiments or cosmological considerations. The region above the solid or dashed lines can be probed by each future experiment. For GW direct detection experiments, solid lines correspond to a background search, and dashed lines correspond to burst detection. Here, "Adv. LIGO+" means the future interferometer network consisting of Advanced LIGO, Advanced Virgo and KAGRA and "current pulsar" means the limit from NANOGrav. The numbered crosses denote the fiducial points studied in Secs. IV B, IV C, and IV D.

IV. CONSTRAINTS ON STRING PARAMETERS FROM FUTURE EXPERIMENTS

In this section, we forecast constraints on the cosmic string parameters expected from various types of future experiments, using the Fisher matrix calculations. We investigate three fiducial models where different types of experiments complement to determine the parameters with better accuracy. Here, we include only string parameters $G\mu$, α, p in theoretical parameters θ_i and calculate the Fisher matrix for them. Assuming that the cosmological parameters are determined with sufficient accuracy, we set them to the aforementioned values and do not marginalize the likelihood over them when calculating constraints on the string parameters. Before that, we show the accessible parameter space by current and future experiments.

A. Accessible parameter space of cosmic string search

Figures 4(a)–4(c) show the regions in the $\alpha - G\mu$ plane which are excluded by current experiments or cosmological constraints and those which can be probed by future experiments for $p = 1$, 10^{-1}, and 10^{-2}.[5] We also show the fiducial parameter points which we consider in the following Fisher analysis.

For GW burst, the region above each curve represents the parameter space where bursts from cosmic strings are detectable more than once per year by each detector. The threshold amplitude and the most sensitive frequency $f_{\rm best}$ for each interferometer are $fh = 1.7 \times 10^{-21}$ and $f_{\rm best} = 150$ Hz for current LIGO, $fh = 3.4 \times 10^{-23}$ and $f_{\rm best} = 220$ Hz for Advanced LIGO, $fh = 5.8 \times 10^{-21}$ and $f_{\rm best} = 7.0 \times 10^{-3}$ Hz for eLISA/NGO, and $fh = 1.9 \times 10^{-24}$ and $f_{\rm best} = 0.25$ Hz for BBO/DECIGO. For GW background, the detection threshold is determined whether the amplitude of the background $\Omega_{\rm GW}$ exceeds the sensitivity of the detector at $f_{\rm best}$, which is $\Omega_{\rm GW} = 7.2 \times 10^{-6}$ for current LIGO, $\Omega_{\rm GW} = 4.5 \times 10^{-9}$ for Advanced LIGO, and $\Omega_{\rm GW} = 9.2 \times 10^{-17}$ for BBO/DECIGO. We assume that if the lowest frequency of GWs emitted by strings, $f_{lc} \sim (\alpha t_0)^{-1}$, where t_0 is the present age of the universe, is lower than $f_{\rm best}$, the GWs cannot be detected either as a background or burst. The vertical cutoff on the left side of the curves for eLISA/NGO and BBO/DECIGO corresponds to the value of α which gives $f_{lc} = f_{\rm best}$.[6]

For the latest pulsar timing experiment, we use the constraint on $\Omega_{\rm GW}$ from NANOGrav. The parameter space is excluded if strings predict the GW background larger

[5]Similar figures can be found in other papers, such as Ref. [13]. Our results in Fig. 4 are similar to those in other papers, but ours tend to be somewhat larger, because of the difference in the string network model and the parameters which contains theoretical uncertainty, such as the prefactor of Eq. (9).

[6]If we take into account the fact that each interferometer has sensitivity over some frequency range, GWs may be detectable even if $f_{lc} > f_{\rm best}$. This may slightly expand the accessible region for large $G\mu$.

than $\Omega_{\rm GW} = 1.9 \times 10^{-8}$ at $f = 1/(5\ \text{years})$. Here, we assume that NANOGrav cannot detect GWs if $f_{lc} > 1/(5\ \text{years})$, which corresponds to the vertical line at the left. For SKA, we show the region where SNR exceeds 4.

We also show the cosmological constraints from CMB and big bang nucleosynthesis (BBN). The constraint is derived from the fact that the energy density of the GW background must be small at the last scattering and BBN, so as not to distort the fluctuations of the CMB or not to change abundance of various nuclei. The CMB constraint is $\int \Omega_{\rm GW}(f) d\ln f < 1.4 \times 10^{-5}$ at the last scattering [99] and the BBN constraint is $\int \Omega_{\rm GW}(f) d\ln f < 1.6 \times 10^{-5}$ at the epoch of BBN [13,100]. The lower limit of the integral is determined by the lowest frequency of the GWs emitted by largest and youngest loops at the time of CMB and BBN. The upper limit is the frequency of GWs emitted by the earliest loops, which we assume to be formed at the end of the friction domination, when the temperature of the Universe is $\sim\sqrt{G\mu}$.

From Figs. 4(a)–4(c), we find that, for large α, current and future pulsar timing experiments are powerful to search for cosmic strings. On the other hand, pulsar timing experiments cannot access to small α, and other types of experiments, such as the direct detection by interferometers or CMB measurement help to set constraints. In the following subsections, we investigate future constraints on the cosmic string parameters from the different types of experiments by choosing parameter sets indicated in Fig. 4(a).

B. Case 1: $G\mu = 10^{-9}$, $\alpha = 10^{-9}$, $p=1$—ground-based interferometers and pulsar timing experiments

First, we consider the case for $G\mu = 10^{-9}$, $\alpha = 10^{-9}$, $p = 1$. In this case, α is large enough for GWs to be detected in the frequency range of pulsar timing experiments. For such a value of α, the tension is already severely constrained and $G\mu = 10^{-9}$ is the maximum value allowed by current pulsar timing constraints. Because of the small tension, we do not expect detection of the string signature by future CMB experiments. However, we instead expect future pulsar timing experiments such as SKA and the ground-based interferometers will detect GWs from strings.

For this parameter set, future interferometers can detect 168 rare bursts with $\rho > 4$, where we assume a 3-year run of the interferometer network consisting of Advanced LIGO, Advanced Virgo and KAGRA. However, the GW background is not large enough to be detected at $f \sim 10^2$ Hz. In contrast, a 10-year observation by SKA can detect the GW background with $\rho \sim 33$. We show the burst rate $dR/d\ln h$ estimated at $f = 220$ Hz, the most sensitive frequency of the ground-based interferometers, as a function of burst amplitude in Fig. 5(a). We also show the spectrum $\Omega_{\rm GW}$ in Fig. 5(b). The plateau region of the spectrum seen in Fig. 5(b) corresponds to GWs emitted in the radiation-dominated era, and the bump in the low frequency region corresponds to those emitted after matter-radiation equality. Since the energy density of GWs is diluted compared with the total energy density after matter-radiation equality, the GWs emitted in the radiation-dominated era are more suppressed compared to that emitted recently, and this makes background detection at high frequencies difficult.

In Figs. 6(a)–6(c), we show the expected constraints on the string parameters from the burst detection by the ground-based interferometers and the GW background detection by SKA, estimated by Fisher matrix calculations. Since the constraints from SKA alone are quite weak, we only show the combined constraints in the figure. One can see SKA slightly improve the constraints when it is combined to the constraint from the ground-based interferometers. This is because the constraints from pulsar timing and interferometer experiments have different directions of parameter degeneracy.

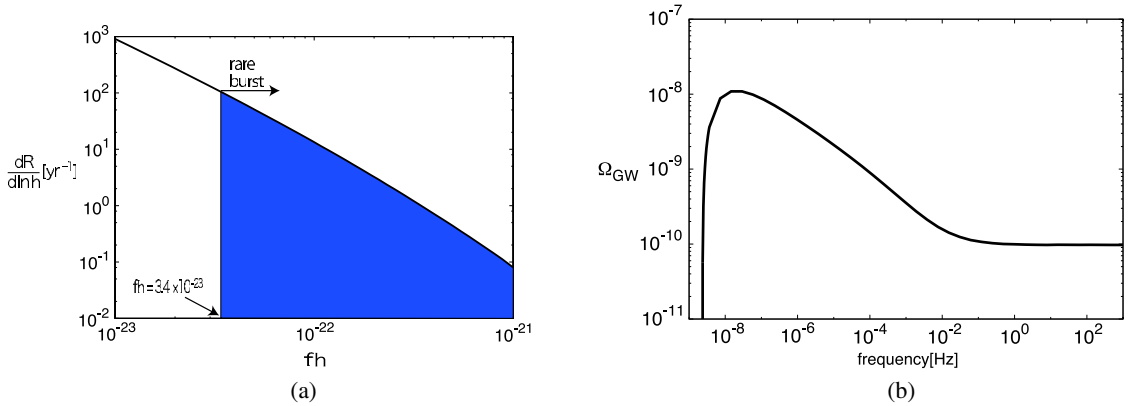

FIG. 5 (color online). (a) The burst rate at $f = 220$ Hz. The bursts in the blue region are detectable as rare bursts by the future ground-based interferometer network. (b) The background spectrum GW. The burst rate at $f = 220$ Hz and the background spectrum $\Omega_{\rm GW}$ for $G\mu = 10^{-9}$, $\alpha = 10^{-9}$, $p = 1$.

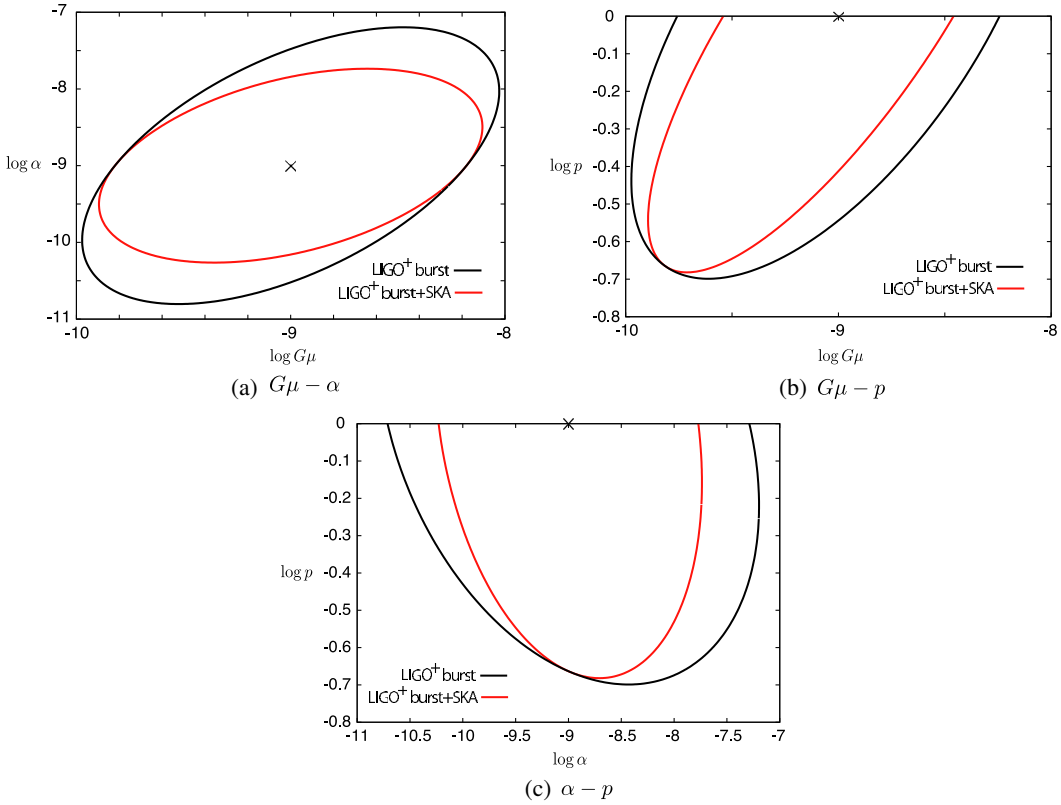

(a) $G\mu - \alpha$ (b) $G\mu - p$ (c) $\alpha - p$

FIG. 6 (color online). Marginalized 2σ constraints on cosmic string parameters shown in the $G\mu - \alpha$, $G\mu - p$ and $\alpha - p$ planes. The fiducial parameter set, denoted by the black cross, is taken to be $G\mu = 10^{-9}$, $\alpha = 10^{-9}$, $p = 1$. The solid black line represents the constraints from the burst detection alone by the ground-based interferometer network consisting of Advanced LIGO, Advanced Virgo and KAGRA. The red line represents the combined constraints from the burst detection and the GW background measurement by SKA.

Let us briefly discuss the parameter degeneracy. In this parameter set, $\alpha < \Gamma G\mu$, so loops evaporate soon after its formation by emitting GWs of frequency $f \sim (\alpha t)^{-1}$, where t is the time of the GW emission. We provide the rough estimates of the parameter degeneracy in $dR/d\ln h$ and $\Omega_{\rm GW}$ for $\alpha < \Gamma G\mu$ in the appendix. For burst detection, the bursts whose amplitude is comparable to the sensitivity of the ground-based interferometers, $fh \sim 3.4 \times 10^{-23}$, are in the range of $h_{3,2} < h < h_{3,3}$ of Eq. (A1), where $fh_{3,2} = 2.3 \times 10^{-27}$ and $fh_{3,3} = 2.2 \times 10^{-22}$ in this case. So the parameter degeneracy of the burst rate is $\propto (G\mu)^{3/8}\alpha^{-3/4}p^{-1}$. Here, $h_{3,2}$ and $h_{3,3}$ are the corresponding amplitude to characterize when the bursts are emitted (for details, see the appendix or Ref. [20]). For example, bursts who have amplitude of $h_{3,2} < h < h_{3,3}$ are emitted between the matter-radiation equality and $z \simeq 1$. The rough estimate of the background spectrum is given by Eq. (A2). For the GW background measurement by SKA, the second term dominates in Eq. (A2), so the parameter degeneracy is $\propto G\mu\alpha^{-1/3}p^{-1}$.[7]

[7]Note that the direction of the degeneracy seen in the figures does not directly correspond to the parameter dependence described here, since the shown constraints are marginalized over the other parameter.

In this fiducial model, eLISA/NGO can also detect GW bursts from strings. Figure 7(a) shows the burst rate at the most sensitive frequency, $f = 7 \times 10^{-3}$ Hz. In the case of eLISA/NGO, the detectable bursts correspond to the case of $h > h_{3,3}$ of Eq. (A1), where $fh_{3,3} = 6.9 \times 10^{-21}$ for $f = 7 \times 10^{-3}$ Hz. Such bursts are emitted recently at $z \lesssim 1$. In Figs. 7(b)–7(d), we show the constraints expected from a 3-year run of eLISA/NGO, which makes 1.4×10^4 burst detections with $\rho > 4$. One can clearly see eLISA/NGO can provide much stronger constraints than ground-based interferometers and SKA. And, of course, BBO/DECIGO will determine the parameters with a significant accuracy. Our Fisher calculation indicates the expected errors on the parameters are $\mathcal{O}(0.1)\%$.

C. Case 2: $G\mu = 10^{-7}$, $\alpha = 10^{-16}$, $p = 1$—ground-based interferometers and CMB experiments

Next, we study the case where $G\mu = 10^{-7}$, $\alpha = 10^{-16}$, $p = 1$. In this case, α is extremely small, so pulsar timing experiments cannot detect GWs from strings. This means that the tension is not constrained strongly by the current pulsar timing experiments and, if $G\mu \sim 10^{-7}$ which is still allowed by current CMB and LIGO experiments, we can expect future CMB experiments to find string signatures.

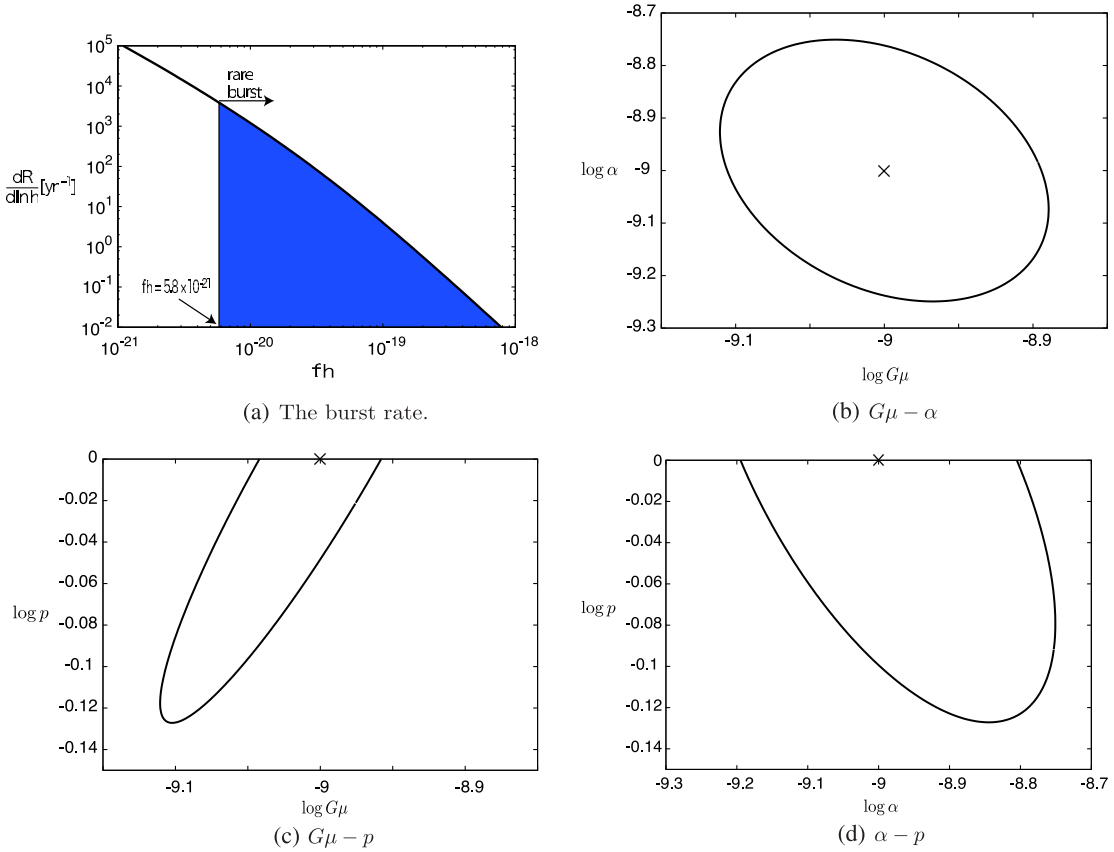

(a) The burst rate. (b) $G\mu - \alpha$ (c) $G\mu - p$ (d) $\alpha - p$

FIG. 7 (color online). (a) The burst rate at $f = 7 \times 10^{-3}$ Hz for $G\mu = 10^{-9}$, $\alpha = 10^{-9}$, $p = 1$. (b), (c), (d) Marginalized 2σ constraints from eLISA on cosmic string parameters in $G\mu - \alpha$, $G\mu - p$ and $\alpha - p$ planes, respectively. The black cross represents the fiducial point.

Also, we can expect both burst and background detection by future ground-based interferometers. The ground-based interferometers will detect 1.8×10^5 rare bursts with $\rho > 4$ and the GW background with $\rho \simeq 187$, where we again assume a 3-year run of the world-wide interferometer network. We show the burst rate at $f = 220$ Hz in Fig. 8(a) and the background spectrum $\Omega_{\rm GW}$ in Fig. 8(b).

In Figs. 9(a)–9(c), we show the constraints on the string parameters from the CMB observation and the burst and GW background detection by the ground-based interferometers. For the GW background, we use the weak signal approximation, Eq. (36), to calculate the Fisher matrix. For CMB, we consider the constraints from Planck and CMBpol. We derive the constraints from CMBpol

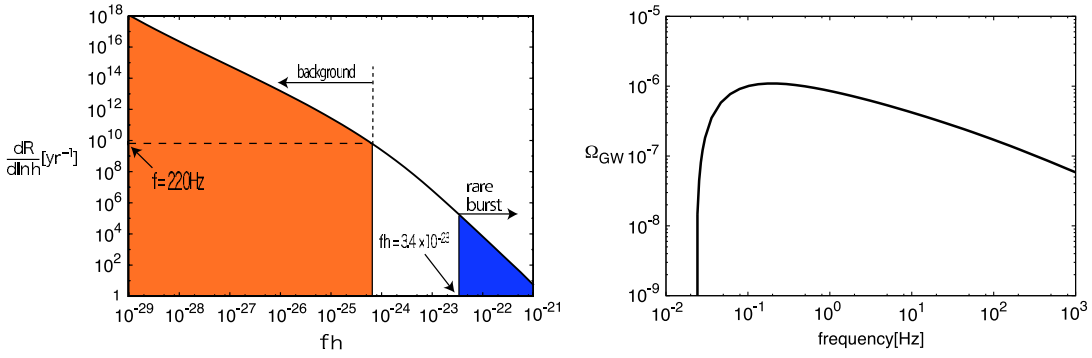

(a) (b)

FIG. 8 (color online). Same as Fig. 5 but for $G\mu = 10^{-7}$, $\alpha = 10^{-16}$, $p = 1$.

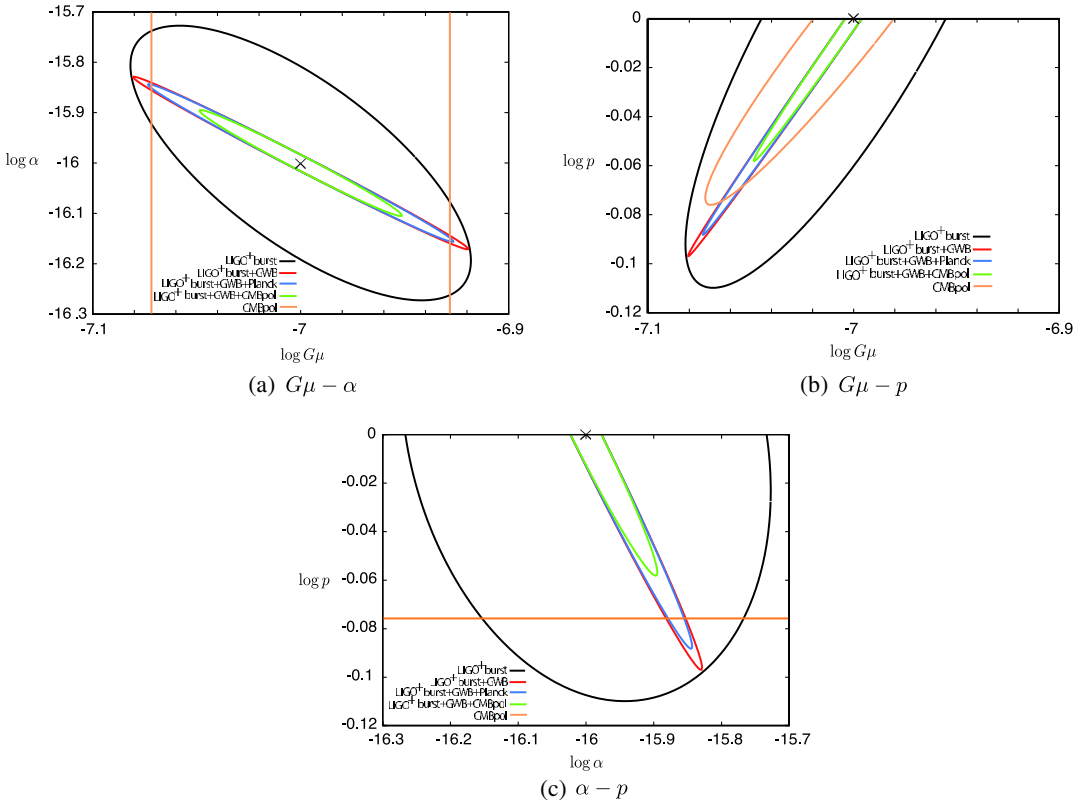

(a) $G\mu - \alpha$ (b) $G\mu - p$ (c) $\alpha - p$

FIG. 9 (color online). Marginalized 2σ constraints on cosmic string parameters shown in the $G\mu - \alpha$, $G\mu - p$ and $\alpha - p$ planes. The fiducial parameter set, denoted by the black cross, is taken to be $G\mu = 10^{-7}$, $\alpha = 10^{-16}$, $p = 1$. The solid black line represents the constraints from the burst detection by the interferometer network consisting of Advanced LIGO, Advanced Virgo and KAGRA alone. The red line represents the combined constraints from the burst detection and the GW background measurement by the interferometer network. The blue or green lines are the constraints from combination of interferometers and Planck or CMBpol, respectively. The orange lines are the constraint from CMBpol alone.

neglecting the lensing effect. The results are not significantly affected by including the lensing effect, as discussed in Sec. III D.

In this case, loops are extremely short-lived. The bursts whose amplitude is comparable to the sensitivity of the ground-based interferometers, $fh \sim 3.4 \times 10^{-23}$, correspond to $h > h_{3,3}$ in Eq. (A1), where $fh_{3,3} = 4.7 \times 10^{-25}$ in this case. These bursts are emitted recently at $z \lesssim 1$. Therefore, for the burst detection, the direction of the parameter degeneracy is $\propto (G\mu)^2 \alpha^{1/3} p^{-1}$. The background spectrum is again expressed by Eq. (A2). The bumplike spectrum in Fig. 8(b) corresponds to the second term in Eq. (A2), which represents GWs emitted recently, and its parameter dependence is $\propto G\mu\alpha^{-1/3}p^{-1}$. CMB measurements provide information on infinite strings, which is characterized by only $G\mu$ and p, and do not contain information on α. The overall amplitude of CMB spectra is proportional to $(G\mu)^2$ and decreasing p leads to enhancement of the amplitude and the change of the spectral shape as explained in Sec. III. We numerically find that the dominant contribution to the Fisher matrix comes from the temperature spectrum around $1000 \lesssim l \lesssim 2000$. For such values of l, $C_l^{\mathrm{TT,str}}$ is roughly proportional to p^{-2}, as shown in Fig. 2(b). Therefore, the parameter degeneracy of the CMB constraint is $\propto (G\mu)^2 p^{-2}$.

D. Case 3: $G\mu = 10^{-14}$, $\alpha = 10^{-13}$, $p = 1$—BBO/DECIGO

Finally, we study the case where $G\mu = 10^{-14}$, $\alpha = 10^{-13}$, $p = 1$. For this small value of $G\mu$, only BBO/DECIGO can detect string signals. In this case, BBO/DECIGO detects 35 rare bursts with $\rho > 4$ in a 3-year run and measures the GW background with very high SNR, $\rho \simeq 510$. We show the burst rate estimated at the best frequency of BBO/DECIGO, $f = 0.25$ Hz, in Fig. 10(a) and the background spectrum in Fig. 10(b).

Figures 11(a)–11(c) show the expected constraints on the string parameters from the burst detection and the background measurement by a 3-year run of BBO/DECIGO. Here, we use the exact formula of the Fisher matrix for the GW background, Eq. (35), because of the high SNR. The background measurement provides stronger constraints than burst detection. However, the constraints from background measurement intrinsically have strong parameter degeneracies, since the information is practically only one Ω_{GW} at $f = f_{\mathrm{best}}$. Thus, although

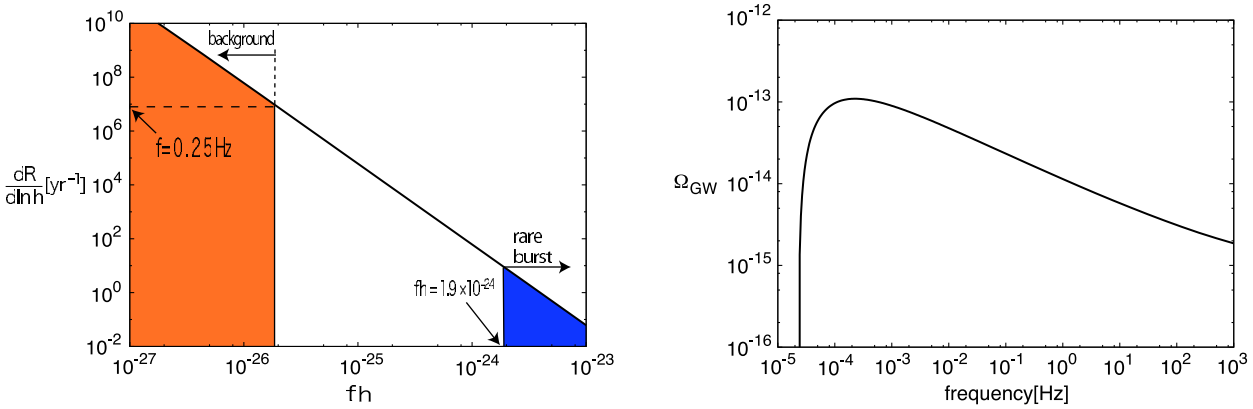

FIG. 10 (color online). Same as Fig. 5 but for $G\mu = 10^{-14}$, $\alpha = 10^{-13}$, $p = 1$.

constraints from the burst detection are weak because of the small number of detectable events, it dramatically tightens the errors when combined with the constraints from the background detection. This is again thanks to the difference in the parametric dependencies.

In this parameter set, loops are marginally short-lived. The bursts detectable by BBO/DECIGO are emitted recently, $z < 1$, and their rate is expressed by the case of $h > h_{3,3}$ of Eq. (A1), where $fh_{3,3} = 4.5 \times 10^{-28}$. So the parameter degeneracy is $\propto (G\mu)^2 \alpha^{1/3} p^{-1}$. The

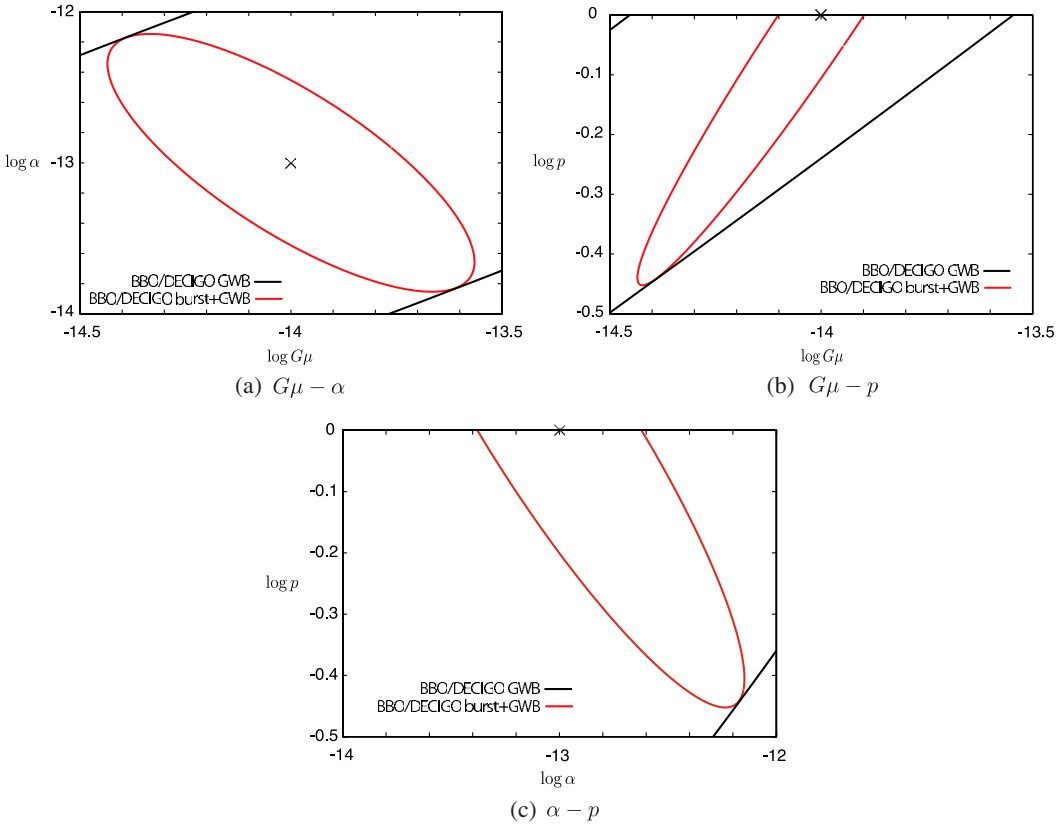

FIG. 11 (color online). The 2σ constraints from BBO/DECIGO on cosmic string parameters in the $G\mu - \alpha$, $G\mu - p$ and $\alpha - p$ planes. The black line shows the marginalized 2σ constraints from background measurement alone. The red line represents the combined constraints from burst detection and background measurement. The fiducial parameter set, denoted by the black cross, is taken to be $G\mu = 10^{-14}$, $\alpha = 10^{-13}$, $p = 1$.

background spectrum around $f = 0.25$ Hz corresponds to GWs emitted at $z < 1$ and is roughly expressed by the second term of Eq. (A2), whose parameter dependence is $\propto G\mu\alpha^{-1/3}p^{-1}$.

V. SUMMARY

Among many types of cosmic string signatures, gravitational waves from cosmic string loops and CMB fluctuations induced by infinite strings are important and future experiments will help to test the existence of cosmic strings. If detected, we may even be able to extract information on the nature of cosmic strings. In this paper, we extend our previous work which investigated the constraints on the string parameters from future ground-based GW experiments. In addition to the ground-based interferometers, this paper has investigated constraints from space-borne interferometers, pulsar timing arrays and CMB experiments. Furthermore, we have studied the combination of information from these observations.

Each experiment sheds light on the different aspect of cosmic strings and gives us different information on strings. More technically speaking, the constraints from different experiments have different parameter degeneracies. CMB experiments probe infinite strings through their gravitational effects on the background photons, while GW interferometers and pulsar timing experiments probe string loops by detecting GWs emitted from them. Among GW experiments, each of them targets a different frequency band; ground-based interferometers detect GWs of $f \sim 220$ Hz, space-borne ones probe those of $f \sim 10^{-4}$ to 0.1 Hz and pulsar timing experiments are sensitive to those of $f \sim 10^{-8}$ Hz. GWs of different frequency are emitted at different epoch of the Universe and provide us with independent information. Besides, different types of GW observations, the burst detection and the background measurement, provide different information on cosmic strings. These are the reasons why we can break the parameter degeneracies by combining these experiments and obtain better constraints on cosmic string parameters.

In this paper, we have studied three different fiducial models, where different types of experiments help each other to constrain the string parameters. The first case is $G\mu = 10^{-9}$, $\alpha = 10^{-9}$, $p = 1$, where both future GW interferometers and pulsar timing such as SKA can detect GWs from cosmic strings. We also calculated constraints from eLISA/NGO and found that it is more efficient to constrain string parameters than the pulsar timing and ground-based experiments. The second case is $G\mu = 10^{-7}$, $\alpha = 10^{-16}$, $p = 1$, where both future GW interferometers and CMB experiments can detect string signatures. The third case is $G\mu = 10^{-14}$, $\alpha = 10^{-13}$, $p = 1$, where the tension is so small that only ultimate space-borne interferometers such as BBO and DECIGO can detect string signatures. We have shown that future GW interferometers, especially space-borne ones, are very powerful to investigate cosmic strings not only because of their extreme sensitivity but also because they can probe strings in two different ways, the background measurement and the burst detection.

Finally, we should note that, in the case where we can determine the parameters with a very good accuracy, uncertainties in the string network model become more important. In that case, further theoretical study will be needed to perform analysis with more accurate modeling, or precise measurements of cosmic string GWs by future space-borne interferometers may even be able to shed light on the theoretical uncertainties in the string evolution.

ACKNOWLEDGMENTS

K. M. and T. S. would like to thank the Japan Society for the Promotion of Science for financial support. This work is supported by the Grant-in-Aid for Scientific Research from the Ministry of Education, Science, Sports, and Culture (MEXT), Japan, No. 23340058 (S. K.), No. 24740149 (S. K.), No. 23740179 (K. T.), No. 24111710 (K. T.), and No. 24340048 (K. T.).

APPENDIX: PARAMETER DEPENDENCE OF THE BURST RATE AND THE GW BACKGROUND SPECTRUM

In this Appendix, we provide rough estimates of the burst rate $dR/d\ln h$ and the GW background spectrum $\Omega_{\rm GW}$ to understand the dependence of these quantities on the cosmic string parameters. We concentrate on the case of $\alpha < \Gamma G\mu$, where loops are short-lived, since this case applies to all the fiducial models investigated in Sec. IV. For other cases, see the appendices of Ref. [20].

In this case, $\alpha < \Gamma G\mu$, the burst rate is given by

$$\frac{dR}{d\ln h}(f,h) \sim \begin{cases} (G\mu)^{6/5}\alpha^{-1/5}\gamma_r^{-2}\left(\frac{\Omega_m}{\Omega_r}\right)^{-11/10} f^{-18/5} t_0^{-12/5} h^{-11/5}; \\ G\mu\alpha^{-1} f^{-3} t_0^{-2}\left(\frac{\Omega_m}{\Omega_r}\right)^{-1/2} \equiv h_{3,1} < h < G\mu\alpha^{2/3} f^{-4/3} t_0^{-1/3}\left(\frac{\Omega_m}{\Omega_r}\right)^{-4/3} \equiv h_{3,2} \\ (G\mu)^{3/8}\alpha^{-3/4}\gamma_m^{-2} f^{-5/2} t_0^{-17/8} h^{-11/8}; h_{3,2} < h < G\mu\alpha^{2/3} f^{-4/3} t_0^{-1/3} \equiv h_{3,3} \\ (G\mu)^2\alpha^{1/3}\gamma_m^{-2} f^{-14/3} t_0^{-8/3} h^{-3}; h > h_{3,3}. \end{cases} \tag{A1}$$

Bursts in the range of $h_{3,1} < h < h_{3,2}$, $h_{3,2} < h < h_{3,3}$, and $h > h_{3,3}$ are emitted in the radiation-dominated era, in the matter-dominated era, and at $z \ll 1$, respectively. The burst rate for $h < h_{3,1}$ is suppressed strongly.

The background spectrum is given by

$$\Omega_{\rm GW}(f) \sim G\mu\gamma_r^{-2}\frac{\Omega_r}{\Omega_m} + G\mu\gamma_m^{-2}\alpha^{-1/3}t_0^{-1/3}f^{-1/3}. \quad \text{(A2)}$$

Here, the first term is the contribution from GWs emitted in the radiation-dominated era and the second one represents GWs emitted recently. Note that the former has smaller amplitude than the latter by the factor of Ω_r/Ω_m, since the energy density of GWs decays faster than the total energy density in the matter-dominated era.

[1] T. W. B. Kibble, J. Phys. A **9**, 1387 (1976).
[2] A. Vilenkin and E. P. S. Shellard, *Cosmic Strings and Other Topological Defects* (Cambridge University Press, Cambridge, England, 1994).
[3] S. Sarangi and S. H. H. Tye, Phys. Lett. B **536**, 185 (2002).
[4] N. T. Jones, H. Stoica, and S. H. H. Tye, Phys. Lett. B **563**, 6 (2003).
[5] G. Dvali and A. Vilenkin, J. Cosmol. Astropart. Phys. 03 (2004) 010.
[6] A. Vilenkin, Phys. Lett. **107B**, 47 (1981).
[7] C. J. Hogan and M. J. Rees, Nature (London) **311**, 109 (1984).
[8] R. R. Caldwell and B. Allen, Phys. Rev. D **45**, 3447 (1992).
[9] R. R. Caldwell, R. A. Battye, and E. P. S. Shellard, Phys. Rev. D **54**, 7146 (1996).
[10] T. Damour and A. Vilenkin, Phys. Rev. Lett. **85**, 3761 (2000).
[11] T. Damour and A. Vilenkin, Phys. Rev. D **64**, 064008 (2001).
[12] T. Damour and A. Vilenkin, Phys. Rev. D **71**, 063510 (2005).
[13] X. Siemens, V. Mandic, and J. Creighton, Phys. Rev. Lett. **98**, 111101 (2007).
[14] M. R. DePies and C. J. Hogan, Phys. Rev. D **75**, 125006 (2007).
[15] M. Kawasaki, K. Miyamoto, and K. Nakayama, Phys. Rev. D **81**, 103523 (2010).
[16] S. Olmez, V. Mandic, and X. Siemens, Phys. Rev. D **81**, 104028 (2010).
[17] P. Binetruy, A. Bohe, C. Caprini, and J.-F. Dufaux, J. Cosmol. Astropart. Phys. 06 (2012) 027.
[18] P. Binetruy, A. Bohe, T. Hertog, and D. A. Steer, Phys. Rev. D **82**, 126007 (2010).
[19] A. Bohe, Phys. Rev. D **84**, 065016 (2011).
[20] S. Kuroyanagi, K. Miyamoto, T. Sekiguchi, K. Takahashi, and J. Silk, Phys. Rev. D **86**, 023503 (2012).
[21] D. Sigg (LIGO Scientific Collaboration), Classical Quantum Gravity **25**, 114041 (2008).
[22] T. Accadia *et al.*, Classical Quantum Gravity **28**, 114002 (2011).
[23] K. Kuroda (LCGT Collaboration), Classical Quantum Gravity **27**, 084004 (2010).
[24] P. Amaro-Seoane *et al.*, arXiv:1201.3621.
[25] E. S. Phinney *et al.*, *Big Bang Observer Mission Concept Study* (NASA, 2003).
[26] S. Kawamura, M. Ando, N. Seto, S. Sato, T. Nakamura, K. Tsubono, N. Kanda, T. Tanaka *et al.*, Classical Quantum Gravity **28**, 094011 (2011).
[27] R. N. Manchester, AIP Conf. Proc. **983**, 584 (2008).
[28] R. D. Ferdman, R. van Haasteren, C. G. Bassa, M. Burgay, I. Cognard, A. Corongiu, N. D'Amico, G. Desvignes *et al.*, Classical Quantum Gravity **27**, 084014 (2010).
[29] R. van Haasteren, Y. Levin, G. H. Janssen, K. Lazaridis, M. K. B. W. Stappers, G. Desvignes, M. B. Purver, A. G. Lyne *et al.*, Mon. Not. R. Astron. Soc. **414**, 3117 (2011); **425**, 1597 (2012).
[30] F. Jenet, L. S. Finn, J. Lazio, A. Lommen, M. McLaughlin, I. Stairs, D. Stinebring, J. Verbiest *et al.*, arXiv:0909.1058.
[31] P. B. Demorest, R. D. Ferdman, M. E. Gonzalez, D. Nice, S. Ransom, I. H. Stairs, Z. Arzoumanian, A. Brazier *et al.*, arXiv:1201.6641.
[32] http://www.skatelescope.org.
[33] N. Kaiser and A. Stebbins, Nature (London) **310**, 391 (1984).
[34] J. R. Gott III, Astrophys. J. **288**, 422 (1985).
[35] U. Seljak, U.-L. Pen, and N. Turok, Phys. Rev. Lett. **79**, 1615 (1997).
[36] L. Pogosian and T. Vachaspati, Phys. Rev. D **60**, 083504 (1999).
[37] K. Benabed and F. Bernardeau, Phys. Rev. D **61**, 123510 (2000).
[38] L. Pogosian, S. H. H. Tye, I. Wasserman, and M. Wyman, Phys. Rev. D **68**, 023506 (2003); **73**, 089904(E) (2006).
[39] U. Seljak and A. Slosar, Phys. Rev. D **74**, 063523 (2006).
[40] N. Bevis, M. Hindmarsh, M. Kunz, and J. Urrestilla, Phys. Rev. Lett. **100**, 021301 (2008).
[41] N. Bevis, M. Hindmarsh, M. Kunz, and J. Urrestilla, Phys. Rev. D **76**, 043005 (2007).
[42] L. Pogosian and M. Wyman, Phys. Rev. D **77**, 083509 (2008).
[43] M. Kawasaki, K. Miyamoto, and K. Nakayama, Phys. Rev. D **82**, 103504 (2010).
[44] R. Battye and A. Moss, Phys. Rev. D **82**, 023521 (2010).
[45] N. Bevis, M. Hindmarsh, M. Kunz, and J. Urrestilla, Phys. Rev. D **82**, 065004 (2010).
[46] D. Yamauchi, K. Takahashi, Y. Sendouda, C.-M. Yoo, and M. Sasaki, Phys. Rev. D **82**, 063518 (2010).
[47] P. Mukherjee, J. Urrestilla, M. Kunz, A. R. Liddle, N. Bevis, and M. Hindmarsh, Phys. Rev. D **83**, 043003 (2011).

[48] Planck Collaboration, arXiv:astro-ph/0604069.
[49] D. Baumann *et al.* (CMBPol Study Team Collaboration), AIP Conf. Proc. **1141**, 10 (2009).
[50] S. Foreman, A. Moss, and D. Scott, Phys. Rev. D **84**, 043522 (2011).
[51] D. P. Bennett and F. R. Bouchet, Phys. Rev. Lett. **60**, 257 (1988); **63**, 2776 (1989); Phys. Rev. D **41**, 2408 (1990).
[52] B. Allen and E. P. S. Shellard, Phys. Rev. Lett. **64**, 119 (1990).
[53] G. R. Vincent, M. Hindmarsh, and M. Sakellariadou, Phys. Rev. D **56**, 637 (1997).
[54] V. Vanchurin, K. D. Olum, and A. Vilenkin, Phys. Rev. D **74**, 063527 (2006).
[55] C. Ringeval, M. Sakellariadou, and F. Bouchet, J. Cosmol. Astropart. Phys. 02 (2007) 023.
[56] C. J. A. P. Martins and E. P. S. Shellard, Phys. Rev. D **73**, 043515 (2006).
[57] K. D. Olum and V. Vanchurin, Phys. Rev. D **75**, 063521 (2007).
[58] J. J. Blanco-Pillado, K. D. Olum, and B. Shlaer, Phys. Rev. D **83**, 083514 (2011).
[59] X. Siemens, K. D. Olum, and A. Vilenkin, Phys. Rev. D **66**, 043501 (2002).
[60] J. Polchinski and J. V. Rocha, Phys. Rev. D **74**, 083504 (2006).
[61] F. Dubath, J. Polchinski, and J. V. Rocha, Phys. Rev. D **77**, 123528 (2008).
[62] V. Vanchurin, Phys. Rev. D **77**, 063532 (2008).
[63] L. Lorenz, C. Ringeval, and M. Sakellariadou, J. Cosmol. Astropart. Phys. 10 (2010) 003.
[64] http://www.sfu.ca/~levon/cmbact.html.
[65] E. Komatsu *et al.* (WMAP Collaboration), Astrophys. J. Suppl. Ser. **192**, 18 (2011).
[66] A. Avgoustidis and E. P. S. Shellard, Phys. Rev. D **73**, 041301 (2006).
[67] K. Takahashi, A. Naruko, Y. Sendouda, D. Yamauchi, C.-M. Yoo, and M. Sasaki, J. Cosmol. Astropart. Phys. 10 (2009) 003.
[68] C. J. A. P. Martins and E. P. S. Shellard, Phys. Rev. D **54**, 2535 (1996).
[69] C. J. A. P. Martins and E. P. S. Shellard, Phys. Rev. D **65**, 043514 (2002).
[70] R. A. Battye, J. Robinson, and A. Albrecht, Phys. Rev. Lett. **80**, 4847 (1998).
[71] A. Lewis, A. Challinor, and A. Lasenby, Astrophys. J. **538**, 473 (2000).
[72] http://camb.info/.
[73] M. Tegmark, A. Taylor, and A. Heavens, Astrophys. J. **480**, 22 (1997).
[74] X. Siemens, J. Creighton, I. Maor, S. R. Majumder, K. Cannon, and J. Read, Phys. Rev. D **73**, 105001 (2006).
[75] B. P. Abbott *et al.* (LIGO Scientific Collaboration), Phys. Rev. D **80**, 062002 (2009).
[76] M. I. Cohen, C. Cutler, and M. Vallisneri, Classical Quantum Gravity **27**, 185012 (2010).
[77] J. S. Key and N. J. Cornish, Phys. Rev. D **79**, 043014 (2009).
[78] N. J. Cornish and L. J. Rubbo, Phys. Rev. D **67**, 022001 (2003); **67**, 029905(E) (2003).
[79] B. Abbott *et al.* (LIGO Collaboration), Phys. Rev. D **69**, 102001 (2004).
[80] L. Baggio *et al.* (AURIGA and LIGO Scientific Collaborations), Classical Quantum Gravity **25**, 095004 (2008).
[81] L. S. Finn and A. N. Lommen, Astrophys. J. **718**, 1400 (2010).
[82] B. Allen and J. D. Romano, Phys. Rev. D **59**, 102001 (1999).
[83] H. Kudoh, A. Taruya, T. Hiramatsu, and Y. Himemoto, Phys. Rev. D **73**, 064006 (2006).
[84] A. Nishizawa, A. Taruya, K. Hayama, S. Kawamura, and M. a. Sakagami, Phys. Rev. D **79**, 082002 (2009).
[85] V. Corbin and N. J. Cornish, Classical Quantum Gravity **23**, 2435 (2006).
[86] N. Seto, Phys. Rev. D **73**, 063001 (2006).
[87] B. Abbott *et al.* (LIGO Scientific Collaboration), Phys. Rev. D **69**, 122004 (2004).
[88] F. B. Estabrook and H. D. Wahlquist, Gen. Relativ. Gravit. **6**, 439 (1975).
[89] M. V. Sazhin, Sov. Astron. **22**, 36 (1978).
[90] S. Detweiler, Astrophys. J. **234**, 1100 (1979).
[91] D. R. Lorimer and M. Kramer, *Handbook of Pulsar Astronomy* (Cambridge University Press, Cambridge, England, 2005).
[92] F. A. Jenet, G. B. Hobbs, K. J. Lee, and R. N. Manchester, Astrophys. J. **625**, L123 (2005).
[93] R. W. Hellings and G. S. Downs, Astrophys. J. **265**, L39 (1983).
[94] A. Sesana and A. Vecchio, Classical Quantum Gravity **27**, 084016 (2010).
[95] M. Zaldarriaga, D. N. Spergel, and U. Seljak, Astrophys. J. **488**, 1 (1997).
[96] L. Knox, Phys. Rev. D **52**, 4307 (1995).
[97] C. Dvorkin, M. Wyman, and W. Hu, Phys. Rev. D **84**, 123519 (2011).
[98] R. Keisler, C. L. Reichardt, K. A. Aird, B. A. Benson, L. E. Bleem, J. E. Carlstrom, C. L. Chang, H. M. Cho *et al.*, Astrophys. J. **743**, 28 (2011).
[99] T. L. Smith, E. Pierpaoli, and M. Kamionkowski, Phys. Rev. Lett. **97**, 021301 (2006).
[100] R. H. Cyburt, B. D. Fields, K. A. Olive, and E. Skillman, Astropart. Phys. **23**, 313 (2005).